Geochimica et Cosmochimica Acta
Manuscript Draft

Manuscript Number: GCA-D-17-00784

Title: Halogens and noble gases in chlorite and garnet peridotites formed by serpentinite dehydration: Implications for seawater subduction and the origin of mantle neon

Article Type: Article

Abstract: Halogens and noble gases were investigated in secondary peridotites formed by serpentinite dehydration reactions (and preserved in ophiolites) to improve constraints on the fates of noble gases and halogens during subduction zone metamorphism. Both whole rock and mineral separates where investigated to identify the dominant mineral hosts of these elements. New samples including high grade (olivine-bearing) antigorite serpentinites and granofels textured chlorite harzburgites from Cerro del Almirez (Betic Cordillera); and a chlorite harzburgite and garnet peridotite from Cima di Gagnone (Swiss Alps); were selected to complement previous studies of low grade chrysotile-serpentinites that retain features of oceanic serpentinisation (IODP samples; Monte Nero, Northern Apennines; Erro Tobbio, Western Alps) and subducted eclogite facies antigorite-serpentinites (Erro Tobbio, Western Alps).
The data show that the 40Ar/36Ar ratios of chrysotile- and antigorite-serpentinites and their dehydrated peridotite equivalents range from ~296-390 in rocks from Erro Tobbio to ~340-600 in rocks from Cerro del Almirez, and to ~600-1100 in rocks from Cima di Gagnone. The variation of 40Ar/36Ar between localities is independent of metamorphic grade but broadly correlated with variation in other radiogenic isotopes (206Pb/204Pb and 87Sr/86Sr) suggesting that excess 40Ar in ophiolitic serpentinites and their dehydrated equivalents was derived from terrigenous sediments in the different subduction zones.
The high compatibilities of noble gases and F in chlorite, and the involvement of fluids derived from sedimentary units in the subducting slab, are suggested to explain the enrichment of chlorite-harzburgites in Ne relative to Ar and F relative to Cl. The 20Ne/36Ar ratios of chlorite harzburgites from both Cerro del Almirez and Cima di Gagnone are much greater than seawater, suggesting that even though subducted atmospheric Ne is a minor component in the Earth's mantle, subduction of atmospheric Ne in dehydrated serpentinites could be sufficiently important to explain how the mantle acquired a 20Ne/22Ne ratio of less than the primordial Solar composition.
The garnet peridotite from Cima di Gagnone records the final and complete dehydration of serpentinite. Based on the analysis of mineral separates minimally affected by retrogression (marked by garnet breakdown and the appearance of Cl-rich hornblende), nominally anhydrous garnet peridotite retains Cl, Br, I and noble gas concentrations up to an order of magnitude higher than average depleted mantle. Furthermore, garnet peridotites preserve Br/Cl and I/Cl ratios fairly close to mantle values, consistent with dehydrated serpentinised lithosphere as a major source of deeply subducted seawater-derived volatiles in the Earth's mantle.

Halogens and noble gases in chlorite and garnet peridotites formed by serpentinite dehydration: Implications for seawater subduction and the origin of mantle neon

M.A. Kendrick[1,2]*, M. Scambelluri[3], J. Hermann[4] and J.A Padrón-Navarta[5]

*corresponding author; mark.kendrick@anu.edu.au

1 – Research School of Earth Sciences, Australian National University, Acton 2601, Australia.

2 – School of Earth Sciences, University of Melbourne, Victoria 3010, Australia.

3– Dipartimento di Scienze della Terra, Ambiente e Vita, Università di Genova, Italy

4 – Institute of Geological Sciences, University of Bern, Switzerland

5 – Géosciences Montpellier, Université de Montpellier, Campus Triolet cc060, Place Eugène Bataillon 34095, Montpellier cedex05, France

Published in Geochimica et Cosmochimica Acta 15 August 2018, Volume 235; P 285-304
https://doi.org/10.1016/j.gca.2018.03.024
Link to publisher version https://www.sciencedirect.com/science/article/pii/S00167037183018

Abstract. Halogens and noble gases were investigated in secondary peridotites formed by serpentinite dehydration reactions (and preserved in ophiolites) to improve constraints on the fates of noble gases and halogens during subduction zone metamorphism. Both whole rock and mineral separates where investigated to identify the dominant mineral hosts of these elements. New samples including high grade (olivine-bearing) antigorite serpentinites and granofels textured chlorite harzburgites from Cerro del Almirez (Betic Cordillera); and a chlorite harzburgite and garnet peridotite from Cima di Gagnone (Swiss Alps); were selected to complement previous studies of low grade chrysotile-serpentinites that retain features of oceanic serpentinisation (IODP samples; Monte Nero, Northern Apennines; Erro Tobbio, Western Alps) and subducted eclogite facies antigorite-serpentinites (Erro Tobbio, Western Alps).

The data show that the $^{40}Ar/^{36}Ar$ ratios of chrysotile- and antigorite-serpentinites and their dehydrated peridotite equivalents range from ~296-390 in rocks from Erro Tobbio to ~340-600 in rocks from Cerro del Almirez, and to ~600-1100 in rocks from Cima di Gagnone. The variation of $^{40}Ar/^{36}Ar$ between localities is independent of metamorphic grade but broadly correlated with variation in other radiogenic isotopes ($^{206}Pb/^{204}Pb$ and $^{87}Sr/^{86}Sr$) suggesting that excess ^{40}Ar in ophiolitic serpentinites and their dehydrated equivalents was derived from terrigenous sediments in the different subduction zones.

The high compatibilities of noble gases and F in chlorite, and the involvement of fluids derived from sedimentary units in the subducting slab, are suggested to explain the enrichment of chlorite-harzburgites in Ne relative to Ar and F relative to Cl. The $^{20}Ne/^{36}Ar$ ratios of chlorite harzburgites from both Cerro del Almirez and Cima di Gagnone are much greater than seawater, suggesting that even though subducted atmospheric Ne is a minor component in the Earth's mantle, subduction of atmospheric Ne in dehydrated serpentinites could be sufficiently important to explain how the mantle acquired a $^{20}Ne/^{22}Ne$ ratio of less than the primordial Solar composition.

The garnet peridotite from Cima di Gagnone records the final and complete dehydration of serpentinite. Based on the analysis of mineral separates minimally affected by retrogression (marked by garnet breakdown and the appearance of Cl-rich hornblende), nominally anhydrous garnet peridotite retains Cl, Br, I and noble gas concentrations up to an order of magnitude higher than average depleted mantle. Furthermore, garnet peridotites preserve Br/Cl and I/Cl ratios fairly close to mantle values, consistent with dehydrated serpentinised lithosphere as a major source of deeply subducted seawater-derived volatiles in the Earth's mantle.

1. Introduction

The halogens and noble gases represent volatile elements that are depleted in the mantle and strongly concentrated in Earth's surface reservoirs of the atmosphere, seawater and sediments (Kendrick et al., 2017; Ozima and Podosek, 2002). As a result, halogens and noble gases represent powerful elements for tracking the subduction of seawater-derived volatiles into the mantle (Chavrit et al., 2016; Holland and Ballentine, 2006; Kendrick et al., 2017; Kobyashi et al., 2017; Sumino et al., 2010). Recent studies have suggested that up to ~90% of non-radiogenic Ar, Kr and Xe and most of the heavy halogens (Cl, Br, I) have subducted origins in the Earth's mantle (Caracausi et al., 2016; Holland and Ballentine, 2006; Holland et al., 2009; Kendrick et al., 2017; Mukhopadhyay, 2012). However, relatively few studies have investigated the combined behaviour of multiple halogens and/or noble gases during prograde metamorphism (John et al., 2011; Kendrick et al., 2015; 2011; Page et al., 2016), with much of what we do know about the behaviour of these elements during metamorphism based on investigations of chlorine and excess ^{40}Ar alone (e.g. Arnaud and Kelley, 1995; Kelley, 2002; Philippot et al., 1998; Scaillet, 1996; Scambelluri et al., 2004a; 1997). The current study addresses this gap in our knowledge by investigating all the noble gases (He, Ne, Ar, Kr, Xe) and halogens (F, Cl, Br, I) in a suite of chlorite and garnet peridotites formed by eclogite facies metamorphism of seafloor serpentinites (Cannaò et al., 2015; Marchesi et al., 2013; Scambelluri et al., 2015; 2014).

The investigation of noble gases and halogens in serpentinites and their metamorphosed equivalents is important because no other major subduction zone lithology is more enriched in seawater-derived Cl or H_2O (Schmidt and Poli, 1998). Furthermore, previous work has shown that serpentinites are strongly enriched in a range of other fluid mobile elements including noble gases and B, which are derived mainly from seawater (e.g. Kendrick et al., 2013b; Scambelluri et al., 2004b; 1997), and in some cases a number of

82 elements including iodine, arsenic and antimomy, which are usually associated with marine
83 sediments (e.g. Cannaò et al., 2015; Deschamps et al., 2012; Hattori and Guillot, 2007;
84 Kendrick et al., 2013b; Peters et al., 2017; Scambelluri et al., 2015). The presence of
85 sediment-like signatures in serpentinites can be explained by the involvement of sedimentary
86 pore waters in serpentinisation reactions (John et al., 2011; Kendrick et al., 2013b; 2011),
87 which are likely to be particularly important at the slab bend where sediments overly deep
88 fractures into the oceanic lithosphere (Ranero et al., 2003) and in subduction channels
89 underlying forearc environments (Bostock et al., 2002; Deschamps et al., 2013; Scambelluri
90 et al., 2015). An implication of serpentinites carrying 'sedimentary' signatures is that
91 aqueous fluids produced by serpentine breakdown reactions in subarc environments might be
92 able to contribute toward the 'sedimentary signature' of some arc lavas (Kendrick et al.,
93 2014; Scambelluri et al., 2015). Peridotites formed by dehydration of serpentinites have also
94 been suggested as an important component of the HIMU mantle reservoir and the principal
95 lithology enabling subduction of noble gases and halogens into the deep mantle (Kendrick et
96 al., 2017; 2011).

97 The current study aims to further constrain the fate of noble gases and halogens
98 during the partial and complete dehydration of serpentinites and builds on previous work that
99 characterised the noble gas and halogen content of seafloor serpentinites and their
100 metamorphosed equivalents from Erro Tobbio in Italy and Cerro del Almirez in Spain (Fig 1;
101 John et al., 2011; Kendrick et al., 2013b; 2011; Scambelluri et al., 2004b; 1997). We provide
102 noble gas and halogen (Cl, Br, I) data for new lithologies that are key for understanding the
103 fates of noble gases and halogens in dehydrating serpentinites and we utilise SHRIMP for the
104 measurement of F in a selection of the new and old samples. The new lithologies investigated
105 include: i) antigorite-serpentinites from Cerro del Almirez, which are more closely related to
106 chlorite harzburgites from this locality, than the antigorite-serpentinites investigated

previously (John et al., 2011; Kendrick et al., 2011); ii) Granofels textured chlorite harzburgites from Cerro del Almirez (Padron-Navarta et al., 2015), which complement previous analyses of chlorite harzburgites with spinifex-like textures (Kendrick et al., 2011); and iii) we selected a chlorite harzburgite and garnet peridotite from Cima di Gagnone, which is the only known locality where garnet peridotites have been produced by the final dehydration of serpentinites (Fig 1). The unique nature of the Cima di Gagnone garnet peridotite means it provides important information about the nature of dehydrated lithosphere subducted into the deep mantle (Evans and Trommsdorff, 1978; Scambelluri et al., 2015; 2014).

2. Geological setting and samples

The study utilises data from a variety of seafloor serpentinites recovered by IODP drilling operations (Kendrick et al., 2013b; Kodolányi et al., 2012), as well as serpentinites and related rocks collected from ophiolite localities including: Monte Nero in the Northern Apennines (John et al., 2011; Scambelluri et al., 2004b), Erro Tobbio in the Ligurian western Alps (Scambelluri et al., 1995; 1997), Cerro del Almirez in the Betic Cordillera of Spain (Garrido et al., 2005; López Sanchez-Vizcaino et al., 2009; 2005; Padron-Navarta et al., 2011; Puga et al., 1999; Scambelluri et al., 2004a; Trommsdorff et al., 1998) and Cima di Gagnone in the Swiss Alps (Evans and Trommsdorff, 1978; Cannaò et al., 2015; Scambelluri et al., 2015; 2014). The samples and locations have been described in detail previously, but some important steps in the samples prograde metamorphism are highlighted below (Fig 1).

Initial serpentinisation is recorded in the seafloor serpentinites and selected chrysotile serpentinites and serpentinised peridotites from Monte Nero and Erro Tobbio. The antigoritisation of chrysotile (Kodolányi and Pettke, 2011) and the first breakdown of

antigorite by the reaction: antigorite + brucite => olivine + H_2O, which releases ~2 wt. % H_2O is recorded by antigorite serpentinites at Erro Tobbio and Cerro del Almirez (Scambelluri et al., 2004b). The final breakdown of antigorite by the reaction: antigorite => olivine + enstatite + chlorite + H_2O, which releases ~5-10 wt. % H_2O is recorded by chlorite harzburgites at both Cerro del Almirez and Cima di Gagnone (Evans and Trommsdorff, 1978; Padron-Navarta et al., 2013; Scambelluri et al., 2001; 2014; Trommsdorff et al., 1998). The chlorite harzburgites at Cerro del Almirez are divided into two textural types, which reflect different rates of reaction progress and fluid escape, one has brown spinifex-like olivine and the second type has a granofels texture (Figs 2a and b; Padron-Navarta et al., 2011). In addition, chlorite-rich veins from this locality are related to the escape of antigorite breakdown fluids. The final dehydration of chlorite harzburgites by the reaction: chlorite + enstatite ± diopside => garnet + olivine + H_2O, which releases ~1-5 wt. % H_2O is recorded by garnet peridotites at a single outcrop (Mg160) at Cima di Gagnone (Evans and Trommsdorff, 1978; Scambelluri et al., 2015; 2014).

Olivine in secondary peridotites formed by serpentine dehydration is easily distinguished from mantle olivine by different major and trace element composition, the presence of Ti-clinohumite defects, or by the presence of ilmenite laths formed after Ti-clinohumite in olivine (Fig 2f; Hermann et al., 2007; Puga et al., 1999; Risold et al., 2001). Fluid inclusions associated with the escape of fluids from dehydrating serpentinites are preserved in olivine veins at Erro Tobbio, and in the nominally anhydrous secondary olivine, enstatite and garnet in samples from both Cerro del Almirez and Cima di Gagnone (Fig 2f; Scambelluri et al., 2004b; 2015; 1997). The fluid inclusions at Erro Tobbio have high salinities of >40 wt. % salt and are preserved intact (Scambelluri et al., 1997). In contrast, fluid inclusions in samples from Cerro del Almirez and Cima di Gagnone have been desiccated by the escape of H^+ ions and/or reaction with the host mineral, but they retain

156 solutes including heavy noble gases representative of the originally trapped fluids (Kendrick
157 et al., 2011; Scambelluri et al., 2004b; 2015). Some photomicrographs of representative
158 textures and fluid related inclusions are shown in Fig 2.

159 **3. Methods**

160 Halogens (F, Cl, Br and I) and noble gases (He, Ne, Ar, Kr and Xe) were measured in
161 whole rock samples and mineral separates (0.2-1 mm size fraction) using a variety of
162 techniques: i) the heavy halogens and noble gases (Cl, Br, I, Ar, Kr and Xe) were measured
163 in irradiated samples by the noble gas method at the University of Melbourne; ii) the
164 distribution of Cl in sample Mg160 was then investigated in a thin section using the JEOL
165 8530F plus Field Emission Electron Microprobe at the Centre of Advanced Microscopy at the
166 Australian National University (ANU); iii) fluorine was measured in mineral separates and
167 flux glasses prepared from whole rock powders using the SHRIMP-II at the ANU; and iv)
168 noble gases including He and Ne as well as Ar, Kr and Xe were measured in non-irradiated
169 sample chips at the ANU.

170

171 ***3.1 Halogens (Cl, Br, I) by the noble gas method and electron microprobe***

172 The noble gas method based on measurement of irradiation-produced noble gas proxy
173 isotopes for the halogens, has sub-ppm detection limit for Cl and sub-ppb detection limits for
174 Br and I (Kendrick, 2012; Kendrick et al., 2013a). It was applied to high purity mineral
175 separates and crushed samples (not powders) approximating whole rocks.

176 The samples were ultrasonically washed in distilled water and acetone and 23-56 mg
177 sized portions were packed in Al-foil and placed in silica glass irradiation canisters along
178 with the ^{40}Ar-^{39}Ar flux monitor Hb3gr (Roddick, 1983) and 3 scapolite gems (Kendrick,
179 2012; Kendrick et al., 2013a). The samples were irradiated in two batches: Almirez

antigorites were included in irradiation UM#44 on the 27th February 2011, and the chlorite and garnet peridotites were included in irradiation UM#53 on the 28th November 2012. Irradiation UM#44 in position 5c of the McMaster reactor, had a duration of 42 hours and received a total neutron fluence of 1.2×10^{19} neutrons cm^{-2} with a thermal/fast neutron ratio of 2.7. Irradiation UM#53 in a central position of the USGS Triga reactor, had a duration of 80 hours and received a total neutron fluence of 7×10^{18} neutrons cm^{-2} with a thermal/fast neutron ratio of 0.8.

The irradiated samples were returned to the noble gas laboratory and analysed within 1 year of irradiation. The samples were placed in Sn-foil packets in an ultra-high vacuum sample holder and baked at ~120 °C for 24 hours to achieve ultra-high vacuum. Each sample was successively dropped into the tantalum resistance furnace and noble gases were extracted in 20 minute heating steps, encompassing a low temperature step (300 or 400 °C) and a high temperature step (1500 or 1600 °C). The extracted gases were purified using a Ti-foil bulk getter at 700 °C and a series of three SAES getters over a period of 1 hour. The purified noble gases were then expanded into the MAP 215-50 noble gas mass spectrometer, and analysed for irradiation-produced and naturally occurring isotopes of Ar, Kr and Xe. The measurements were made in static vacuum in 9 cycles of peak jumping over a period of ~50 minutes.

The abundances of Cl, Br, I, K and Ca were calculated from signals of irradiation-produced $^{38}Ar_{Cl}$, $^{80}Kr_{Br,}$ $^{128}Xe_{I,}$ $^{39}Ar_{K}$ and $^{37}Ar_{Ca}$ based on mass spectrometer sensitivity determined via daily air calibrations and noble gas production ratios ($^{38}Ar_{Cl}$/Cl, $^{80}Kr_{Br}$/Br, $^{128}Xe_{I}$/I, $^{39}Ar_{K}$/K, $^{37}Ar_{Ca}$/Ca) determined from the irradiation monitors (Kendrick, 2012; Kendrick et al., 2013a). Analytical precision is at the 1-2% level for element ratios, but the long term reproducibility of elemental abundances, relevant for comparing analyses of

samples included in different irradiations and different techniques is estimated as 10% (2σ) (see (Kendrick et al., 2013a).

The JEOL 8530 plus electron microprobe was subsequently used to investigate the distribution of Cl in sample Mg160. The analytical conditions for EPMA included an accelerating potential of 15 keV, beam current of 20 nA and a 8 μm spot size. Counting times during the main analytical session were 10 seconds for the majority of elements and 30 seconds for Cl, which gave a calculated Cl detection limit of ~30 ppm. Scapolite BB1 with 3.1 wt % Cl was used as the Cl calibration standard (Kendrick, 2012). Durango apatite analysed as an unknown gave a Cl concentration of 0.45 wt %, which is within the previously reported range (Marks et al., 2012; Nadzri et al., 2017).

3.2 Fluorine by SHRIMP-II

The SHRIMP-II housed at the ANU was used to measure F signals in individual grains of chlorite, garnet, olivine and pyroxene separated from the chlorite harzburgites and garnet peridotite. In addition, SHRIMP-II was used to measure F in Li-metaborate glasses produced by flux melting various whole rock sample powders. This was undertaken to test if SHRIMP could be used to measure F in whole rocks as well as mineral separates in a single analytical session. Possible matrix affects and F-loss from Li-metaborate glasses was evaluated by preparing Li-metaborate glasses of F-doped MORB and producing a F-doped MORB glass in a piston cyclinder at 1250 °C and 6 kbar. The SHRIMP results for these glasses define a calibration curve (Fig 3), which gives F concentrations of 279 ± 1 ppm in NIST SRM 610 (n = 2), 330 ± 40 ppm in RGM-2 (n = 3, flux glass) and 1150 ppm in JR-1 (flux glass). In comparison, this is within uncertainty of independently calibrated values for the NIST glass (Hoskin, 1999; Kendrick et al., 2017) and brackets values reported for the

228 rock standards (Michel and Villemant, 2003; Balcone-Boissard et al., 2009). Together with
229 the data for whole rocks and mineral separates (below), this demonstrates that matrix affects
230 between the glasses and minerals were <10% and F-loss during preparation of Li-metaborate
231 flux glasses was negligible.

232 Flux glasses were prepared following standard XRF protocols: whole rock powders
233 were mixed with a lithium metaborate flux in a ratio of 1:3 and placed in a platinum crucible.
234 A drop of ammonium nitrate was added to the powder and dried in a furnace at 400 °C for 10
235 minutes. The sample was then placed in a furnace and melted at 1080 °C for 10 minutes
236 during which time it was continuously agitated. The glass was quenched by removal from
237 the furnace and then broken into multiple chips. A Li metaborate glass (with no sample) was
238 prepared as a blank for this procedure and was found to contain a few ppm F meaning that the
239 effective limit for reliable F measurement in whole rocks by this procedure is ~20 ppm,
240 compared to ppm level detection limits in mineral grains. The flux glass chips and mineral
241 separates were mounted in epoxy and polished to a 1 µm finish. The polished mount was
242 cleaned with acetone, dried overnight in a vacuum furnace at 100 °C and given a 10 nm thick
243 gold coat before loading into the SHRIMP II for analysis.

244 The sample mount was held in the SHRIMP-II ultrahigh-vacuum chamber at a
245 potential of 10 kV and targeted with a primary Cs^+ ion beam focused to a ~30 µm spot on the
246 sample. The ion beam generated with a Kimball Physics Cs gun (IGS-4) was 2 nA and had an
247 energy of 5 kV. Charge compensation was achieved by focusing a 2 kV electron beam
248 generated with a Kimball Physics electron gun onto the sample mount. Secondary ^{19}F and ^{18}O
249 released from the sample were measured by Faraday multi-collection (10^{11} and 10^{12}
250 resistors). The instrument was configured to give resolution of 5,000 (1% valley definition).
251 Data was collected over four 20 s integration periods in static mode (total measurement time

80 s). The measured ^{19}F signal was calibrated using ^{18}O as an internal standard and the calibration curve constructed with F-doped Li-metaborate flux glasses (Fig 3).

3.3 Noble gas analysis in non-irradiated samples

Portions of non-irradiated mineral separates (~100-500 mg), and unsorted mineral grains approximating whole rocks, were ultrasonically washed in acetone and distilled water. After drying they were then wrapped in Sn-foil sample packets and loaded into an ultra-high vacuum sample carasol attached to a resistance furnace on the VG5400 noble gas mass spectrometer at the ANU. The non-irradiated samples were baked overnight at >200 °C to achieve ultra-high vacuum and outgassed in a single 30 minute heating step at 1800 °C. The extracted gases were purified using two Ti-foil bulk getters and a SAES getter over a period of at least 2.5 hours. The purified gas was condensed onto a cryogenic head at 33 K and each noble gas was sequentially released and isotopically analysed in the VG 5400 noble gas mass spectrometer. Small corrections were made for instrumental blank and interference of $^{40}Ar^{++}$ on ^{20}Ne and CO_2^{++} on ^{22}Ne. The methods have been described previously by Honda et al. (2004).

4. Results

4.1 Chlorine, Bromine and Iodine

A significant proportion of the irradiation-produced noble gas isotopes used to measure Cl, Br, I, K and Ca were released in the low temperature heating steps of each sample (Table 1). Low temperature release of $^{38}Ar_{Cl}$ can account for as much as ~50% of the total $^{38}Ar_{Cl}$ released from chrysotile-serpentinites and ~20% of $^{38}Ar_{Cl}$ released from antigorite-serpentinites and chlorite harzburgites, but it only accounted for ~1% of the total $^{38}Ar_{Cl}$ released from the garnet peridotite minerals (Table 1). The release pattern is consistent

277 with the presence of loosely bound water soluble halogens in the lowest grade serpentinites
278 (Sharp and Barnes, 2004), and the presence of halogen-bearing fluid inclusions in the chlorite
279 harzburgites, which probably leak at temperatures of 300-400 °C. As the loosely bound
280 halogens account for an important part of the samples total halogen inventory, mineral and
281 whole rock Cl, Br, I, K and Ca concentrations are based on the total $^{38}Ar_{Cl}$, $^{80}Kr_{Br}$, $^{128}Xe_{I}$,
282 $^{39}Ar_{K}$ and $^{37}Ar_{Ca}$ released from each sample in all heating steps (Table 2).

283 The new analyses indicate antigorite-serpentinites from Cerro del Almirez have 160-
284 250 ppm Cl, 200-370 ppb Br and 17-32 ppb I, which encompass a similar range as those
285 previously reported for antigorite-serpentinites from Erro Tobbio (Fig 4; Table 2). In
286 comparison, the chlorite harzburgites from Cerro del Almirez and Cima di Gagnone have
287 lower concentrations of 36-180 ppm Cl, 210-320 ppb Br and 7-30 ppb I (Fig 4; Table 2). The
288 bulk of the Cl in the chlorite harzburgites is hosted by the olivine and opx, presumably in
289 fluid inclusions: the oliv-opx mineral separates (Almirez) contain 170-240 ppm Cl, 220-340
290 ppb Br and 22-29 ppb I, compared with concentrations of 140-150 ppm Cl, 130-200 ppb Br
291 and 42-47 ppb I in the chlorite mineral separates (Fig 4; Table 2).

292 The mineral separates obtained from the Cima di Gagnone garnet peridotite (Mg160)
293 have variable halogen concentrations of 20 ppm Cl in olv-opx, 78 ppm Cl in garnet and an
294 unexpectedly high concentration of 290 ppm Cl in the clinopyroxene separate (Table 2),
295 which contains up to ~10% retrograde amphibole (Fig 5). Based on the modal mineralogy
296 (50 ol: 15 opx; 25 gnt: 10 cpx(+ hbl)), we estimate whole rock concentrations of ~60 ppm Cl,
297 ~250 ppb Br and ~12 ppb I (Table 2). These concentrations are higher than, or similar to the
298 concentrations of Cl, Br and I in the chlorite harzburgite from Cima di Gagnone (Mg31 09-
299 03; Table 2); however, the presence of retrograde amphibole in the clinopyroxene mineral
300 separate means that they are not considered representative of the peak metamorphic mineral
301 assemblage.

Retrograde amphiboles with ~12 wt % CaO and ~0.1-0.5 wt % Cl are found replacing both garnet and clinopyroxene in Mg160 (Figs 5 and 6; Table 3). However, the green colouration and very fine grain size of the retrograde amphibole (ranging from mm-size down to 10's of microns) meant that it was much harder to separate from green clinopyroxene than pink garnet during hand picking. As a result, retrograde amphibole is mainly in the clinopyroxene mineral separate which has a concentration of 290 ppm Cl and ~20 wt. % CaO (Table 2), which is lower than the concentration of ~23 wt. % CaO in pure clinopyroxene (Scambelluri et al., 2014). In contrast, the garnet separate has a Cl concentration of 78 ppm that is still much greater than in the olivine-opx separate with 20 ppm Cl (Table 2), but this cannot be explained by the presence of calcic amphibole, because it has a bulk CaO concentration of 4.1 wt % that is slightly lower than Cima di Gagnone garnet (Scambelluri et al., 2014). Instead, the high Cl content of the garnet is probably explained by the presence of Cl-rich inclusions related to peak metamorphism that have been documented in this mineral previously (Scambelluri et al., 2015).

The original Cl, Br and I contents of the peak metamorphic garnet peridotite are estimated as ~40 ppm Cl, ~170 ppb Br and ~10 ppb I based on the model mineralogy (50 ol: 15 opx; 25 gnt: 10 cpx(+ hbl)), but excluding the contaminated cpx mineral separate (Table 2). The estimated peak metamorphic concentrations of Cl, Br and I are 20-30% lower than in the retrograded sample, and similar to the values measured in the chlorite harzburgite from Cima di Gagnone (Table 2).

4.2 Fluorine

The new F measurements made by SHRIMP-II on individual minerals and flux glasses are comparable with previous whole rock analyses made by combining

pyrohydrolysis and ion chromatography (John et al., 2011). Thirteen chrysotile- and antigorite-serpentinites investigated for F have concentrations of less than the 20 ppm limit for reliable measurement in whole rock flux glasses. However, the chrysotile-serpentinite sample MN5 from Monte Nero and the antigorite-serpentinite sample Alm-94 from Cerro del Almirez were both indicated to have ~20 ppm F (e.g. F close to the detection limit; Table 2). These results are consistent with the previous work, which indicated 1-18 ppm F in serpentinites from Erro Tobbio and 14-30 ppm F in serpentinites from Monte Nero (John et al., 2011).

In contrast with the serpentinite samples, chlorite harzburgites from both Cerro del Almirez and Cima di Gagnone have F concentrations ranging from 36 ppm up to 170 ppm (Table 2). The highest concentration of 170 ppm F obtained in the spinifex-like sample Alm-8 is much higher than the value of 38 ppm F obtained for this sample by John et al. (2011), and is probably explained by the localised presence of Ti-clinohumite in these rocks, which can contain <0.01-2 wt. % F (López Sanchez-Vizcaino et al., 2005; Puga et al., 1999; Scambelluri et al., 2014). Therefore a concentration range of 36-78 ppm F, that excludes Alm 8, is considered more typical of the chlorite harzburgites investigated (Table 2).

SHRIMP analysis of individual minerals from the chlorite harzburgite Al08-16, which has a whole rock concentration of ~49 ppm F, indicates that chlorite with 220-280 ppm F is the dominant F host. In comparison, the olivine contains only 9-28 ppm F and enstatite contains only ~5 ppm F (Table 2). The measured concentrations of F in the whole rock and the mineral separates are consistent with a modal chlorite abundance of 15%, that is close to the value of 21% estimated optically (Padron-Navarta et al., 2011). Consequently, it is suggested that negligible F is hosted in either fluid inclusions or Ti-clinohumite in this sample. The chlorite-rich veins investigated (Alm-13.3 and Alm-11) have F concentrations

of 170-270 ppm F that overlap the concentration ranges of the chlorite mineral separates (Table 2).

The garnet peridotite has a F concentration of 11 ppm calculated from the modal mineral abundances (50 ol: 15 opx; 25 gnt: 10 cpx(+ hbl)) and concentrations of F in individual minerals (Fig 4a). Among the main minerals, garnet has the lowest concentration of 5±1 ppm F, clinopyroxene has the most variable F content with an average of 10±5 ppm and olivine has the highest average F concentration of ~13±2 ppm F (Table 2). Fluorine was also not detected in a flux glass of this sample, reflecting the calculated concentration of 11 ppm that is below the 20 ppm detection limit for flux glasses.

4.3 Noble gases

A very large proportion of the total atmospheric noble gas released from irradiated samples was released in low temperature heating steps at 300-400 °C (Table 1). Low temperature release accounted for as much as 95 % of the total ^{36}Ar released from serpentinites and 30-50% of the total ^{36}Ar released from peridotites (Table 1). The proportion of atmospheric ^{36}Ar to irradiation-produced $^{38}Ar_{Cl}$ was always high in low temperature steps (Table 1), and the gases released at low temperature had uniformly atmospheric $^{40}Ar/^{36}Ar$ ratios. These observations indicate that atmospheric contamination incompletely removed from the sample surfaces by baking at ~120 °C was released in the 300-400 °C heating steps of irradiated samples. Noble gas concentrations determined for irradiated samples are therefore based on the gas released only in high temperature steps, which are minimally affected by atmospheric contamination (Table 4). Noble gas concentrations and $^{40}Ar/^{36}Ar$ ratios obtained for high temperature steps of irradiated samples in this way (Table 4) are comparable with those obtained for non-irradiated samples analysed

374 in a single heating step, but baked at >200 °C before analysis (Table 5), suggesting that both
375 approaches effectively remove atmospheric contamination.

376 The antigorite-serpentinites from Cerro del Almirez have concentrations of 65-
377 750×10^{-15} mol/g ^{36}Ar, which is similar to the range of 90-740×10^{-15} mol/g ^{36}Ar obtained for
378 antigorite-serpentinites from Erro Tobbio (Kendrick et al., 2011) and is significantly lower
379 than the range of 110-$5{,}400\times10^{-15}$ mol/g reported for chrysotile serpentinites (Tables 4 and 5;
380 Fig 7; Kendrick et al., 2013b).

381 The mineral separates obtained from the granofels chlorite harzburgites from Cerro
382 del Almirez have concentrations of 9-640×10^{-15} mol/g ^{36}Ar, encompassing a slightly greater
383 range than reported for spinifex-like rocks from this locality (21-260×10^{-15} mol/g ^{36}Ar;
384 Kendrick et al., 2011). The chlorite harzburgite from Cima di Gagnone (Mg31 09-03) has a
385 concentration of 290×10^{-15} mol/g ^{36}Ar that is also within this range (Fig 7; Tables 4 and 5).
386 Interestingly, the chlorite mineral separates from both Al08-16 and Al10-06 have much
387 higher concentrations of ^{36}Ar (210-640×10^{-15} mol/g) than the olivine-enstatite separates (9.4-
388 78×10^{-15} mol/g), even though it is the olivine-enstatite separates that have the higher Cl
389 concentrations (170-240 ppm), which was attributed to the presence of fluid inclusions in
390 these minerals (section 4.1). These data indicate that while fluid inclusions are a dominant
391 reservoir for heavy halogens in chlorite harzburgites, the mineral structure of chlorite is of
392 equal or slightly greater importance for hosting noble gases (Fig 8).

393 The mineral separates from the garnet peridotite from Cima di Gagnone have variable
394 ^{36}Ar concentrations. The highest ^{36}Ar concentration of 120×10^{-15} mol/g was obtained for the
395 clinopyroxene separate, which contains retrograde amphibole (section 4.1). The garnet and
396 olivine mineral separates have lower ^{36}Ar concentrations of 46×10^{-15} mol/g and 25×10^{-15}
397 mol/g, respectively. A whole rock concentration of 56×10^{-15} mol/g ^{36}Ar was obtained for the
398 538 mg non-irradiated aliquot of sample Mg160, which is slightly higher than that calculated

399 from the modal abundances of the minerals in this rock (cf. Tables 4 and 5). Excluding the
400 clinopyroxene mineral separate, the peak metamorphic concentration could have been as low
401 as ~31×10^{-15} mol/g ^{36}Ar, which remains fifteen times higher than estimated depleted mantle
402 values (Table 5; Holland and Ballentine, 2006).

403 Samples from different localities have ^{40}Ar/^{36}Ar ratios that fall within characteristic
404 ranges and are representative of fluids either originally responsible for serpentinisation or
405 introduced during subduction-zone metamorphism (Kendrick et al., 2013b; 2011): the
406 samples contain only a few ppm of K (Table 2), meaning that *in situ* production of radiogenic
407 ^{40}Ar is negligible in all of the samples analysed (Fig 9), even though K has locally elevated
408 concentrations in retrograde hornblende (Fig 6; Table 3). The serpentinites from Erro
409 Tobbio have ^{40}Ar/^{36}Ar ratios of between the atmospheric or seawater value of 296 and ~390
410 (Fig 10a; Tables 4 and 5). The antigorite-serpentinites and chlorite harzburgites from Cerro
411 del Almirez have ^{40}Ar/^{36}Ar ratios of ~320-650, and the chlorite and garnet peridotites from
412 Cima di Gagnone have the highest ^{40}Ar/^{36}Ar ratios of ~600-1100 (Fig 10a; Tables 4 and 5).
413 The ranges of ^{40}Ar/^{36}Ar at each locality are broadly correlated with the ^{87}Sr/^{86}Sr and
414 ^{206}Pb/^{204}Pb isotope ratios reported for Erro Tobbio, Cerro del Almirez and Cima di Gagnone
415 (Fig 10; Cannaò et al., 2015; 2016; Harvey et al., 2014).

416 All the samples investigated for helium isotopes have ^{3}He below the detection limit
417 but are enriched in ^{4}He relative to air (Table 6); however, as we lack U and Th data on the
418 aliquots analysed, a full discussion of the ^{4}He budget from *in situ* decay and trapping and
419 involving substantial ^{4}He loss from most samples is beyond the scope of this paper. All
420 samples have Ne, Kr and Xe isotope signatures within uncertainty of air and the abundances
421 of atmospheric ^{20}Ne, ^{84}Kr and ^{130}Xe are broadly correlated with ^{36}Ar (below; Fig 7).

422

5. Discussion

The new data provide some important insights on a range of issues including: the origin of serpentinising fluids, how noble gases and halogens are trapped in subduction zone-lithologies, the nature of fluid processes and the behaviour of noble gases and halogens during prograde metamorphism of serpentinites, and localised retrogression (Fig 5). In addition, the data have significant implications for understanding how seawater-derived volatiles might be subducted into the subarc and deep mantle (Kendrick et al., 2017; 2011; Scambelluri et al., 2015) and for interpretation of Earth's accretion which is partly constrained by the mantle's $^{20}Ne/^{22}Ne$ ratio (Ballentine et al., 2005; Moreira and Charnoz, 2016; Mukhopadhyay, 2012; Péron et al., 2017; Trieloff et al., 2000). Our discussion focuses successively on each of these interrelated themes.

5.1 The origin of serpentinising fluids

The low grade seafloor and ophiolite serpentinites investigated in this study and John et al. (2011) have F concentrations between 1 and 30 ppm, with the majority containing <20 ppm F that encompasses a range of concentrations similar to average depleted mantle with 12 ± 2 ppm F (Fig 4a; Table 4). In comparison, Cl is strongly enriched in serpentinites relative to the average depleted mantle concentration of ~5 ppm (Fig 4; Table 2). The strong enrichment of Cl and Cl/F is consistent with serpentinisation by seawater-derived fluids because seawater contains ~1.9 wt. % Cl but only 1.3 ppm F. Consequently, seawater can only be invoked as a significant source of F if serpentinisation occurred at a very high water/rock ratios.

The relative compatibilities of Cl, Br and I in serpentinites are not known, but all the low grade chrysotile serpentinites investigated have I/Cl intermediate of the mantle and sediments, with a range of Br/Cl and I/Cl ratios that overlaps sedimentary pore waters (Fig

11). The similarity of pore water and serpentinite Br/Cl and I/Cl signatures suggests organic matter in sediments is a likely source of I and Br in many serpentinites (John et al., 2011; Kendrick et al., 2013b; 2011). As carbonate present in organic-rich marine sediments can contain more than 1000 ppm of F (Rude and Aller, 1991), sediments also represent a possible source of F enrichment in serpentinites (Table 2; John et al., 2011). However, it should be noted that F has a low mobility at temperatures of <200 °C (Seyfried and Ding, 1995) and a concentration similar to seawater in sedimentary pore fluids (Gieskes et al., 2002).

The relationship between the ranges of $^{40}Ar/^{36}Ar$ ratios of samples from each of the subducted ophiolite localities and the radiogenic isotopes, suggests additional interaction with sediment-derived fluids during subduction. The serpentinites and peridotites from all the subducted ophiolites investigated have $^{40}Ar/^{36}Ar$ ratios of significantly greater than the atmospheric/seawater value of 296, and range from 310-390 in samples from Erro Tobbio to ~1000 in the garnet peridotite from Cima di Gagnone (Figs 9 and 10; Tables 4 and 5). The presence of excess ^{40}Ar in serpentinites could potentially come from either mantle ^{40}Ar outgassed into seawater-derived fluids (or remobilised from igneous crust), or K-bearing sediments. However, because the ranges of $^{40}Ar/^{36}Ar$ obtained for serpentinite-related samples from each ophiolite are broadly correlated with $^{87}Sr/^{86}Sr$ and $^{206}Pb/^{204}Pb$ (Fig 10), we argue that excess ^{40}Ar was probably derived from K and Rb bearing sediments. The reverse argument also implies sediments are likely to have contributed Sr to serpentinite-related samples with $^{87}Sr/^{86}Sr$ ratios of close to the seawater value of 0.709 (cf. Harvey et al., 2014). Given that terrignous sediments are of greatest importance on continental margins, fluid interaction with K- and Rb-rich terrigenous sediments is most likely to have occurred during subduction, rather than during seafloor serpentinisation.

The serpentinites have ranges of $^{20}Ne/^{36}Ar$, $^{84}Kr/^{36}Ar$ and $^{130}Xe/^{36}Ar$ that are similar to sediments and sedimentary pore waters (Fig 12; Matsuda and Nagoa, 1986; Pitre and Pinti,

2010; Podosek et al., 1980). We believe the $^{20}Ne/^{36}Ar$ enrichment of chlorite harzburgites and garnet peridotites, relative to chrysotile- and antigorite-serpentinites is explained by sedimentary fluid fluxing the subduction channels hosting these rocks. The involvement of high temperature subduction zone fluids would also facilitate mobilisation of F, which is strongly enriched in the chlorite harzburgites compared to serpentinites (Fig 4) and has a low mobility in loer temperature sedimentary pore waters (Gieskes et al., 2002).

5.2 Siting of noble gases and halogens in serpentinites and related rocks

Chrysotile and antigorite are typically very fine grained and do not contain microscopically visible fluid inclusions. The high concentrations of Cl, Br and I in chrysotile-serpentinites therefore suggests that all the halogens can either substitute for the OH-group in chrysotile or are efficiently trapped in the abundant nano-porosity between serpentine minerals (Lafay et al., 2016; Plumper et al., 2012). Vacant ring sites in the serpentine lattice (and other hydrous minerals) have been experimentally demonstrated as important hosts for noble gases (Jackson et al., 2013; 2015) and noble gases could also be stored along grain boundaries or in nano-porosity between serpentine minerals.

In contrast, desiccated fluid inclusions are present in olivine and enstatite formed by antigorite breakdown (e.g. Fig 2f; Scambelluri et al., 2004b; 1997) and could be important reservoirs for subduction of noble gases and halogens into the deeper mantle (Kendrick et al., 2011). Our new data indicate the relative importance of these fluid inclusions is different for noble gases, F and heavy halogens: chlorite in samples Al08-16 and Al10-06 contains very few visible fluid inclusions but it has concentrations of noble gases that are 5-10 times higher, F concentrations that are 10-20 times higher and Cl, Br and I concentrations that are similar to the more abundant olivine and enstatite minerals (Tables 4 and 5). As a result, on a whole rock basis, chlorite with an estimated modal abundance of ~15% is the dominant host of F

and Ne, and of approximately equal importance as fluid inclusions in olivine and enstatite for hosting heavy noble gases (Fig 8).

The high concentration of noble gases in chlorite is consistent with the high compatibility of Ar in other sheet silicates under high pressure metamorphic conditions (Kelley, 2002). Furthermore, the chlorite has slightly higher $^{20}Ne/^{36}Ar$ than the olivine-enstatite (Tables 4 and 5; Figs 8 and 12), which is consistent with preferential storage of light noble gases in ring sites (Jackson et al., 2013). The relatively high concentrations of Br and I in chlorite suggest that halides of these large elements are like F^- and Cl^- able to substitute of the OH-group in chlorite formed under eclogite facies conditions (Table 2). Desiccated fluid inclusions are however, the dominant host of heavy halogens (Cl, Br and I) on a whole rock basis (Fig 8).

5.3 Halogens during subduction and metamorphism

The samples in this study were selected to investigate the progression from chrysotile-serpentinites through antigorite-serpentinites and chlorite harzburgites to garnet peridotites during subduction-related dehydration metamorphism (Fig 1). However, the interpretation of these rock's geochemical signatures must also consider the possibilities that the rocks at each locality had protoliths with important differences and that serpentinites in ophiolites were formed or modified by slab fluids during subduction.

In comparison with the seafloor serpentinites, the high grade antigorite serpentinites, chlorite harzburgites and garnet peridotites have progressively lower concentrations of Cl, Br and I (Fig 4). Furthermore, the metamorphosed serpentinites from all the ophiolites investigated have much lower Br/Cl and I/Cl ratios than forearc serpentinites (Fig 11). This is interpreted to reflect preferential loss of Br and I early in the subduction cycle through the

521 forearc, during the early stages of antigoritisation of chrysotile (Kendrick et al., 2013) and
522 during the reaction, antigorite + brucite => olivine + H_2O (Kendrick et al., 2011). In contrast,
523 the similarity of Br/Cl and I/Cl in antigorite-serpentinites and chlorite harzburgites from
524 Cerro del Almirez, which are characterised by unusually low Br/Cl ratios (Fig 11),
525 demonstrates that Cl, Br and I are not significantly fractionated during the final breakdown of
526 antigorite (cf. Kendrick et al., 2011). These relationships might be explained by the
527 increasing importance of fluid inclusions for hosting halogens in the higher grade rocks
528 because fluid inclusions do not fractionate heavy halogens. The origin of the unusually low
529 Br/Cl ratios in the samples from Cerro del Almirez is uncertain, but it must reflect water-rock
530 reactions and alteration processes unique to this locality (Fig 11).

531 In contrast with the heavy halogens, F is only slightly enriched in chrysotile and
532 antigorite serpentinites, which have <20-30 ppm F, but it is significantly enriched in chlorite
533 harzburgites from Cerro del Almirez and Cima di Gagnone, which have 36-78 ppm F (Fig 4a;
534 Table 2; John et al., 2011). In contrast with John et al. (2011), we suggest that this is unlikely
535 to reflect preferential loss of Cl during subduction zone metamorphic dehydration.
536 Preferential loss of Cl could account for the slightly elevated F/Cl ratios of these rocks, but it
537 cannot explain their high F content (Fig 4a). Instead, the enrichment of F in chlorite
538 harzburgites relative to antigorite serpentinites from Cerro del Almirez (Fig 4a), indicates that
539 either these units had slightly different protoliths with the F enrichment of chlorite
540 harzburgites explained by serpentinisation at very high water/rock ratios, or more likely, F
541 was introduced into the chlorite harzburgite from a neighbouring sedimentary lithology
542 during subduction zone metamorphism (section 5.1).

543 Three lines of reasoning support the introduction of F from neighbouring lithologies
544 during subduction: i) an external F source is favoured by the previous observation that the
545 highest F concentrations in Ti-clinohumite occur adjacent to ophiocarbonates in Almirez

(Puga et al., 1999); ii) the $^{40}Ar/^{36}Ar$ and radiogenic isotopes of the samples favour introduction of a fluid equilibrated with terrigenous sediment (Figs 9, 10 and 12; Marchesi et al., 2013; Cannaò et al., 2015); and iii) F would be more easily mobilised by high temperature subduction zone fluids than low temperature sedimentary pore waters (cf. Gieskes et al., 2002; Seyfried and Ding, 1995).

The peak metamorphic mineral assemblage in the garnet peridotite from Cima di Gagnone has estimated concentrations of <10 ppm F and ~40 ppm Cl (section 5.1). Fluorine probably substitutes for O^{2-} in the nominally anhydrous minerals present (Dalou et al., 2012), whereas the Cl, Br and I are hosted predominantly by desiccated fluid inclusions (Fig 8), which have previously been shown to contain Cl-rich phases (Scambelluri et al., 2015). The garnet peridotite has a F concentration similar to the depleted mantle but contains up to an order of magnitude more Cl, Br and I than the depleted mantle (Fig 4).

5.4 Noble gas loss during prograde metamorphism

The atmospheric noble gas isotopes ^{20}Ne, ^{36}Ar, ^{84}Kr and ^{130}Xe have initial abundances in serpentinites related to their compatibilities in serpentine and abundances in seawater and sediments. The concentrations of noble gases are very broadly correlated with the concentrations of heavy halogens (Fig 13) and become less abundant as the grade of metamorphism is increased and the rock is progressively dehydrated (cf. Figs 1 and Fig 7; Kendrick et al., 2013b; 2011). The progressive decrease in noble gas and halogen concentrations is consistent with these elements being initially stored in the serpentine lattice and then gradually lost with fluids escaping the system during stepwise dehydration (Fig 1). A significant proportion of noble gases remaining in the partially dehydrated rock unit are partitioned into the lattice of chlorite forming after antigorite breakdown (Fig 8); however,

570 fluid inclusions in nominally anhydrous minerals are the dominant host of noble gases in the
571 garnet peridotite. The dual significance of the desiccated fluid inclusions described by
572 Scambelluri et al. (2004a; 2015) is that they provide evidence for noble gases leaving (or
573 fluxing) the rock units during dehydration and they are an important host of noble gases
574 remaining in the nominally anhydrous product of serpentinite dehydration.

575 Despite the overall decrease in noble gas abundance, the $^{20}Ne/^{36}Ar$ increases from
576 values of 0.1-0.11 in chrysotile and antigorite serpentinites to systematically higher values of
577 0.21-0.25 in chlorite harzburgites and garnet peridotites (Figs 7 and 12). The average
578 $^{20}Ne/^{36}Ar$ ratios of the chlorite harzburgites and garnet peridotites are just slightly higher than
579 the 25 °C seawater $^{20}Ne/^{36}Ar$ value of 0.17 (Fig 12).

580 The low $^{20}Ne/^{36}Ar$ of the seafloor serpentinites suggests that serpentinites entering
581 subduction zones, like marine sediments (Matsuda and Nagoa, 1986), are not generally
582 enriched in Ne relative to Ar (Fig 7). However, the enhanced $^{20}Ne/^{36}Ar$ of the subduction
583 zone peridotites provides evidence for interaction with ^{20}Ne-rich sedimentary pore fluids
584 during subduction (Fig 12). Sediment-derived fluids have already been proposed to explain
585 the F enrichment of chlorite harzburgites (section 5.4) and chemical exchange with sediments
586 is required to explain the $^{40}Ar/^{36}Ar$ and radiogenic isotope signatures of high grade
587 serpentinite related rocks (Fig 10; (Cannaò et al., 2015; 2016; Harvey et al., 2014; Marchesi
588 et al., 2013). However, the high $^{20}Ne/^{36}Ar$ of chlorite and garnet peridotites could also be
589 explained by preferential trapping of Ne relative to Ar in chlorite formed by antigorite
590 dehydration. This mechanism is consistent with the high solubility of light noble gases in
591 vacant ring sites (Jackson et al., 2013) and the high $^{20}Ne/^{36}Ar$ of the chlorite compared with
592 olivine and enstatite in samples Al08-16 and Al10-06 (Table 5). Therefore the final
593 characteristics of noble gases subducted into the mantle in dehydrated serpentinites are

shaped by several processes including mineral compatibilities, chemical exchange with neighbouring slab lithology's and dehydration.

5.5 Exhumation and retrogression of sample Mg160

The majority of the samples investigated in this study were chosen specifically because they record peak metamorphic mineral assemblages and have not been affected by retrograde alteration (Fig 1; Kendrick et al., 2011). The halogen and noble gas signatures of most of these rocks appear to be related to the fluids responsible for serpentinisation and subsequent chemical exchange during subduction, with little to no alteration of the signatures during exhumation (section 5.2-5.4). The preservation of seafloor and subduction zone noble gas and halogen signatures is consistent with evidence from other trace elements and radiogenic isotopes. The original noble gas and halogen signatures are probably preserved because exhumation occurs relatively quickly and in the virtual absence of free fluids that would enable efficient gas loss (Kelley, 2002; Sherlock and Kelley, 2002).

The garnet peridotite from Cima di Gagnone is the only sample that was demonstrably influenced by retrograde alteration (Fig 5). Retrograde Cl-rich hornblende was detected in this sample replacing clinopyroxene and garnet and associated with kelyphite rims (Fig 5). The amphibole in Mg160 is estimated to account for <1-2% of the thin section investigated, it ranges in form from grains of 10's of μm in size in kelyphite rims that are clearly secondary in origin (Fig 5a), to examples that are mm-size and appear to be in textural equilibrium with the other peridotite minerals (Figs 5d,g). However, on close inspection some of the larger amphiboles inspected include tiny inclusions of garnet or clinopyroxene that provide evidence for a secondary origin by replacement processes (Figs 5 e,h). The different amphiboles exhibit continuous variation in compositional parameters (Fig 6), irrespective of

618 size and habit that suggests the amphiboles all have a close genetic relationship. Therefore all
619 the amphiboles analysed in the investigated the section of Mg160 are interpreted to have a
620 secondary early retrograde origin.

621 Previous works have reported textural relationships and REE abundance patterns
622 suggesting that at least some of the amphibole present in the Mg160 outcrop has a peak
623 metamorphic origin (Pfiffner and Trommsdorff, 1998; Scambelluri et al., 2014). The
624 different textures reported in hand specimen scale samples from different studies of the
625 Mg160 outcrop are consistent with the known heterogeneity of this outcrop and together with
626 the independent geobarometry of Nimis and Trommsdorff (2001), suggest that the outcrop
627 reached a metamorphic peak straddling the ~3 GPa phase transition between amphibole-free
628 and amphibole-bearing assemblages (Fig 1). Nonetheless, the fact that the current hand
629 specimen is dominated by retrograde amphibole justifies our use of it to estimate peak
630 metamorphic volatile contents by excluding the amphibole (section 4 and Tables 2 and 4).

631 The documentation of retrograde amphibole in this sample is also consistent with the
632 original proposition of Evans and Tromsdorff (1978) that an assemblage of garnet + opx +
633 cpx + olv (assem I) was overprinted by a later assemblage of garnet + opx + cpx + olv + hbl
634 (assem II), in outcrop Mg160 of Cima di Gagnone (below). The kelyphite symplectites
635 record the reaction: garnet => orthopyroxene + spinel, with the stabilisation of spinel
636 representing a pressure drop to below ~1 GPa (Fig 15 of Scambelluri et al., 2014). The
637 presence of Mg-hornblende is interpreted here as indicating the localised infiltration of
638 retrograde aqueous fluids. However, the high Cl content of 0.1-0.4 wt % of the secondary
639 hornblende suggests a very low water/rock ratio: the highest Cl contents were probably
640 acquired as the infiltrating fluid became progressively desiccated by forming the hornblende,
641 with the latest fine grained hornblendes formed from the most saline fluids (Fig 6; Table 3).

642

643 ***5.6 Implications for seawater subduction***

644 Serpentinites are the most H_2O- and Cl-rich of all major subduction zone lithologies and
645 therefore represent major reservoirs for subduction of seawater-derived volatiles into the
646 mantle (Philippot et al., 1998; Scambelluri et al., 1997). The serpentinites and metamorphic
647 peridotites investigated in this study have been subducted to maximum depths of only ~100
648 km (Fig 1; section 5.5; Evans and Trommsdorff, 1978; Scambelluri et al., 2001; 1995; 2004b;
649 2014; Trommsdorff et al., 1998). However, the mineral assemblages investigated are stable
650 over large ranges of pressure and temperature (Fig 1) and evidence from earthquake focal
651 depths suggests that antigorite can be stable to depths as great as 250 km in cold subduction
652 zones (Green II et al., 2010). As a result serpentinites have been widely recognised as an
653 important possible source of fluids in the subarc mantle (Schmidt and Poli, 1998; Kendrick et
654 al., 2014; Scambelluri et al., 2014).

655 The extent to which seawater-derived H_2O, halogens and noble gases could be
656 subducted even more deeply into the mantle beyond the magmatic arc, in metamorphosed
657 serpentinites, is contentious. However, in cold subduction zones where antigorite
658 serpentinites are subducted to sub-arc depths and beyond, the final breakdown of antigorite
659 could contribute fluids enriching back arc basin basalts in H_2O, Cl and I (Kendrick et al.,
660 2014; Sun et al., 2007). Evidence from the SW Pacific indicates that the fluids enriching
661 back arc basins have variable I/Cl, with I/Cl extending above MORB mantle values in some
662 cases but falling short of the extreme ratios observed in sediments, which is potentially
663 consistent with a role for serpentinite breakdown fluids (Kendrick et al., 2014).

664 Subduction of seawater components into the deep mantle beyond the arc and back arc
665 is most likely in cold subduction zones. Furthermore, in units that have an initially low
666 degree of serpentinisation, the water released by antigorite breakdown could conceivably be
667 retained by the production of chlorite within the rock unit (e.g. the unit retains a similar H_2O

content but more of it is altered). If water is subducted deeply enough in hydrous minerals such as chlorite, experimental minerals like phase A (Fig 1), or clinohumite defect structures in olivine (Hermann et al., 2007), then it can eventually be accommodated by solubility in nominally anhydrous minerals. Olivine polymorphs can contain wt. % levels of H_2O in the mantle transition zone (Kohlstedt et al., 1996) and once H_2O, which is the main solvent is safely trapped in these minerals, other fluid mobile elements including noble gases are effectively stranded in the down going subducting slab.

Possible evidence for these processes have recently been identified in the coupled enrichment of H_2O and halogens in some HIMU mantle reservoirs (Kendrick et al., 2017). The trace element signature of HIMU has previously been linked to dehydrated ocean crust (Chauvel et al., 1992; Hofmann, 2003), but the H_2O and halogen enrichment of these reservoirs could be more easily explained if dehydrated ocean crust is associated with H_2O and Cl enriched lithosphere that went through serpentinite dehydration reactions (Kendrick et al., 2017).

5.7 *Implications for Earth's accretion*

The mantle has a $^{38}Ar/^{36}Ar$ ratio indistinguishable from air and non-radiogenic Kr and Xe isotope signatures much closer to the composition of the modern atmosphere than possible primordial end-members (Caracausi et al., 2016; Holland and Ballentine, 2006; Holland et al., 2009; Mukhopadhyay, 2012; Raquin and Moreira, 2009; Trieloff et al., 2000). This has been interpreted as indicating that ~85-90% of the non-radiogenic Ar, Kr and Xe in the Earth's mantle originated through subduction of seawater-derived gases rather than during Earth's accretion (Caracausi et al., 2016; Holland and Ballentine, 2006; Holland et al., 2009; Mukhopadhyay, 2012). In contrast, the similarity of the maximum measured $^{20}Ne/^{22}Ne$ ratio in materials derived from the mantle (~12.5-12.9; Mukhopadhyay, 2012; Yokochi and Marty, 2004) and neon implanted in meteorites (Ne-B), coupled with the low solubility of

neon in seawater, has lead some workers to conclude that subduction of atmospheric Ne is negligible (Holland and Ballentine, 2006; Péron et al., 2016; Péron et al., 2017).

The current results are important for evaluating this theory because they show that secondary peridotites formed by the dehydration of serpentinites acquire $^{20}Ne/^{36}Ar$ ratios of considerably higher than seawater, as a result of chemical exchange between subduction zone lithologies (sections 5.1 and 5.4), which means the argument pertaining to neon solubility in seawater is no longer persuasive.

If neon is subducted into the mantle in serpentinite related lithologies with $^{20}Ne/^{36}Ar$ of 0.1-0.3 (Fig 12), we calculate that based on 90-100% of the total ^{36}Ar in the mantle having a subducted atmospheric origin (Holland and Ballentine, 2006), that the primordial mantle must have had a $^{20}Ne/^{22}Ne$ ratio of 0.3-1.3 higher than the modern mantle (Fig 14). Furthermore, if noble gases were subducted into the mantle in reservoirs with $^{20}Ne/^{36}Ar$ similar to peridotites formed by serpentine dehydration, which we regard as the most likely scenario, then the maximum measured $^{20}Ne/^{22}Ne$ ratios of ~12.9 in Ocean Island Basalts from Iceland and the Galápagos (Mukhopadhyay, 2012; Péron et al., 2016; Yokochi and Marty, 2004), could be explained by mixing primordial mantle neon derived from only the sun (13.4 ± 0.2; Heber et al., 2012) with subducted atmospheric neon (9.8) (Fig 14). We note that a mixed origin of neon from the Sun and implanted in meteorites may be more likely in the MORB mantle, which has lower maximum $^{20}Ne/^{22}Ne$ ratio. However, these calculations show that allowing for minor subduction of atmospheric neon (e.g. ~10% of the total) favours the presence of true Solar neon in the Earth's mantle and therefore the one time existence of an extensive magma ocean on the Early Earth (Mukhopadhyay, 2012; Tucker and Mukhopadhyay, 2014) over alternative chondrite related models (Péron et al., 2016).

6. Conclusions

Noble gases and halogens in seafloor serpentinites and their metamorphosed equivalents in ophiolites record long histories of fluid alteration on the seafloor and metamorphism during subduction with only minor evidence for exhumation-related retrograde alteration or noble gas loss in the samples investigated. As previously concluded for studies of excess ^{40}Ar, the preservation of prograde noble gas signatures is made possible by rapid exhumation in the absence of free fluids. Noble gases and halogens are hosted in serpentinites in the mineral structure, but fluid related inclusions in nominally anhydrous minerals formed by serpentine breakdown become increasingly important with depth.

Seafloor serpentinites have variable noble gas and halogen abundance ratios reflecting serpentinisation by evolved seawater-derived fluids. In many cases, high concentrations of I and Br provide evidence for fluid interaction with marine sediments or the involvement of sedimentary pore waters. Elevated $^{40}Ar/^{36}Ar$ ratios of up to ~1000 that correlate with radiogenic $^{87}Sr/^{86}Sr$ and $^{206}Pb/^{204}Pb$ in serpentinites from ophiolites provide evidence for further modification of serpentinites by interaction with slab fluids derived from sediments during subduction. The strong enrichment of F/Cl in chlorite harzburgites from Cerro del Almirez and the moderate enrichment of $^{20}Ne/^{36}Ar$ in all secondary peridotite from both Cerro del Almirez and Cima di Gagnone provide evidence that slab fluids remobilise F and light noble gases during subduction and that these elements are retained in fluid inclusions and chlorite in the partially dehydrated residues of antigorite breakdown.

Noble gases and halogens become progressively less abundant in serpentinites and their metamorphosed equivalents with increasing levels of dehydration. Br and I are preferentially lost relative to Cl during the initial stages of dehydration, but once fluid inclusion become the dominant hosts for these elements they are no longer fractionated. Noble gases are not strongly fractionated by diffusional mechanisms during metamorphism

but they are redistributed by slab fluids. Nominally anhydrous minerals formed by dehydration reactions retain noble gas and halogen concentrations of greater than average depleted mantle values. Furthermore, despite isotopic evidence for extensive interaction with sediments they have Br/Cl and I/Cl ratios close to mantle values, consistent with the proposed major role of peridotites formed by serpentine dehydration in recycling halogens to the deep mantle. Subduction of seawater-derived volatiles into the deep mantle is estimated to be sufficiently important that it can explain a change in the mantle's $^{20}Ne/^{22}Ne$ isotope signature from a primordial value of similar to the Sun (~13.4), to the current highest measured values of 12.9, meaning that subduction of volatiles exert a major influence on interpretation of mantle noble gas systematics.

Acknowledgements

Dr M.A. Kendrick is supported by an ARC Future Fellowship (FT13 0100141). This work was made possible by the invaluable and expert technical support of Stanislav Szerepanski and Xiaodong Zhang in the noble gas laboratories at Melbourne University and the ANU respectively, and Pete Holden in the ANU SHRIMP laboratory. The authors acknowledge the facilities, and the scientific and technical assistance, of the Australian Microscopy & Microanalysis Research Facility at the Centre of Advanced Microscopy, the Australian National University.

References

Arnaud, N. O. and Kelley, S. P., 1995. Evidence for excess argon during high pressure metamorphism in the Dora Maira Massif (western Alps, Italy), using an ultra-violet laser ablation microprobe 40Ar-39Ar technique. *Contributions to Mineralogy and Petrology* **121**, 1-11.

Balcone-Boissard, H., Michel, A., and Villemant, B., 2009. Simultaneous Determination of Fluorine, Chlorine, Bromine and Iodine in Six Geochemical Reference Materials Using Pyrohydrolysis, Ion Chromatography and Inductively Coupled Plasma-Mass Spectrometry. *Geostandards and Geoanalytical Research* **33**, 477-485.

Ballentine, C. J., Marty, B., Lollar, B. S., and Cassidy, M., 2005. Neon isotopes constrain convection and volatile origin in the Earth's mantle. *Nature* **433**, 33-38.

Bostock, M. G., Hyndman, R. D., Rondenay, S., and Peacock, S. M., 2002. An inverted continental Moho and serpentinization of the forearc mantle. *Nature* **417**, 536-538.

Cannaò, E., Agostini, S., Scambelluri, M., Tonarini, S., and Godard, M., 2015. B, Sr and Pb isotope geochemistry of high-pressure Alpine metaperidotites monitors fluid-mediated element recycling during serpentinite dehydration in subduction mélange (Cima di Gagnone, Swiss Central Alps). *Geochimica et Cosmochimica Acta* **163**, 80-100.

Cannaò, E., Scambelluri, M., Agostini, S., Tonarini, S., and Godard, M., 2016. Linking serpentinite geochemistry with tectonic evolution at the subduction plate-interface: The Voltri Massif case study (Ligurian Western Alps, Italy). *Geochimica et Cosmochimica Acta* **190**, 115-133.

Caracausi, A., Avice, G., Burnard, P. G., Füri, E., and Marty, B., 2016. Chondritic xenon in the Earth's mantle. *Nature* **533**, 82-85.

Chauvel, C., Hofmann, A. W., and Vidal, P., 1992. HIMU EM - The French-Polynesian Connection. *Earth and Planetary Science Letters* **110**, 99-119.

Chavrit, D., Burgess, R., Sumino, H., Teagle, D. A. H., Droop, G., Shimizu, A., and Ballentine, C. J., 2016. The contribution of hydrothermally altered ocean crust to the mantle halogen and noble gas cycles. *Geochimica et Cosmochimica Acta* **183**, 106-124.

Dalou, C. l., Koga, K., Shimizu, N., Boulon, J., and Devidal, J.-L., 2012. Experimental determination of F and Cl partitioning between lherzolite and basaltic melt. *Contributions to Mineralogy and Petrology* **163**, 591-609.

Deschamps, F., Godard, M., Guillot, S., Chauvel, C., Andreani, M., Hattori, K., Wunder, B., and France, L., 2012. Behavior of fluid-mobile elements in serpentines from abyssal to subduction environments: Examples from Cuba and Dominican Republic. *Chemical Geology* **312,** 93-117.

Evans, B. W. and Trommsdorff, V., 1978. PETROGENESIS OF GARNET LHERZOLITE, CIMA-DI-GAGNONE, LEPONTINE ALPS. *Earth and Planetary Science Letters* **40**, 333-348.

Garrido, C. J., Sanchez-Vizcaino, V. L., Gomez-Pugnaire, M. T., Trommsdorff, V., Alard, O., Bodinier, J. L., and Godard, M., 2005. Enrichment of HFSE in chlorite-harzburgite produced by high-pressure dehydration of antigorite-serpentinite: Implications for subduction magmatism. *Geochem. Geophys. Geosyst.* **6**.

Gieskes, J. M., Simoneit, B. R. T., Goodfellow, W. D., Baker, P. A., and Mahn, C., 2002. Hydrothermal geochemistry of sediments and pore waters in Escanaba Trough—ODP Leg 169. *Applied Geochemistry* **17**, 1435-1456.

Green II, H. W., Chen, W.-P., and Brudzinski, M. R., 2010. Seismic evidence of negligible water carried below 400-km depth in subducting lithosphere. *Nature* **467**, 828-831.

Harvey, J., Garrido, C. J., Savov, I., Agostini, S., Padron-Navarta, J. A., Marchesi, C., Sanchez-Vizcaino, V. L., and Gomez-Pugnaire, M. T., 2014. 11B-rich fluids in subduction zones: The role of antigorite dehydration in subducting slabs and boron isotope heterogeneity in the mantle. *Chemical Geology* **376**, 20-30.

Hattori, K. H. and Guillot, S., 2007. Geochemical character of serpentinites associated with high- to ultrahigh-pressure metamorphic rocks in the Alps, Cuba, and the Himalayas: Recycling of elements in subduction zones. *Geochem. Geophys. Geosyst.* **8**, 27.

Heber, V. S., Baur, H., Bochsler, P., McKeegan, K. D., Neugebauer, M., Reisenfeld, D. B., Wieler, R., and Wiens, R. C., 2012. Isotopic mass fractionatio of Solar Wind: Evidence from fast and slow Solar Wind collected by the Genesis Mission. *Astrophysical Journal* **759**.

Hermann, J., Fitz Gerald, J. D., Malaspina, N., Berry, A. J., and Scambelluri, M., 2007. OH-bearing planar defects in olivine produced by the breakdown of Ti-rich humite minerals from Dabie Shan (China). *Contributions to Mineralogy and Petrology* **153**, 417-428.

Hofmann, A. W., 2003. Sampling Mantle Heterogeneity through Oceanic Basalts: Isotopes and Trace Elements. In: Carlson, R. L. (Ed.), *Treatise of Geochemistry Volume 2: The Core and Mantle*. Elsevier Ltd.

Holland, G. and Ballentine, C. J., 2006. Seawater subduction controls the heavy noble gas composition of the mantle. *Nature* **441**, 186-191.

Holland, G., Cassidy, M., and Ballentine, C. J., 2009. Meteorite Kr in Earth's Mantle Suggests a Late Accretionary Source for the Atmosphere. *Science* **326**, 1522-1525.

Honda, M., Phillips, D., Harris, J. W., and Yatsevich, I., 2004. Unusual noble gas compositions in polycrystalline diamonds: preliminary results from the Jwaneng kimberlite, Botswana. *Chemical Geology* **203**, 347-358.

Hoskin, P. W. O., 1999. SIMS determination of mu g g(-1)-level fluorine in geological samples and its concentration in NIST SRM 610. *Geostandards Newsletter-the Journal of Geostandards and Geoanalysis* **23**, 69-76.

Jackson, C. R. M., Parman, S. W., Kelley, S. P., and Cooper, R. F., 2013. Noble gas transport into the mantle facilitated by high solubility in amphibole. *Nature Geosci* **6**, 562-565.

Jackson, C. R. M., Parman, S. W., Kelley, S. P., and Cooper, R. F., 2015. Light noble gas dissolution into ring structure-bearing materials and lattice influences on noble gas recycling. *Geochimica et Cosmochimica Acta* **159**, 1-15.

John, T., Scambelluri, M., Frische, M., Barnes, J. D., and Bach, W., 2011. Dehydration of subducting serpentinite: Implications for halogen mobility in subduction zones and the deep halogen cycle. *Earth and Planetary Science Letters* **308**, 65-76.

Kelley, S., 2002. Excess argon in K-Ar and Ar-Ar geochronology. *Chemical Geology* **188**, 1-22.

Kendrick, M. A., 2012. High precision Cl, Br and I determination in mineral standards using the noble gas method. *Chemical Geology* **292-293**, 116-126.

Kendrick, M. A., Arculus, R. J., Burnard, P., and Honda, M., 2013a. Quantifying brine assimilation by submarine magmas: Examples from the Galápagos Spreading Centre and Lau Basin. *Geochimica et Cosmochimica Acta* **123**, 150-165.

Kendrick, M. A., Arculus, R. J., Danyushevsky, L., Kamenetsky, V. S., Woodhead, J., and Honda, M., 2014. Subduction-related halogens (Cl, Br and I) and H2O in magmatic glasses from Southwest Pacific Backarc Basins. *Earth and Planetary Science Letters* **400**, 165-176.

Kendrick, M. A., Hémond, C., Kamenetsky, V. S., Danyushevsky, L., Devey, C. W., Rodemann, T., Jackson, M. G., and Perfit, M. R., 2017. Seawater cycled throughout Earth's mantle in partially serpentinized lithosphere. *Nat. Geosci.* **10**, 222-228.

Kendrick, M. A., Honda, M., Pettke, T., Scambelluri, M., Phillips, D., and Giuliani, A., 2013b. Subduction zone fluxes of halogens and noble gases in seafloor and forearc serpentinites. *Earth and Planetary Science Letters* **365**, 86-96.

Kendrick, M. A., Honda, M., and Vanko, D. A., 2015. Halogens and noble gases in Mathematician Ridge meta-gabbros, NE Pacific: implications for oceanic hydrothermal root zones and global volatile cycles. *Contributions to Mineralogy and Petrology* **170**, 1-20.

Kendrick, M. A., Scambelluri, M., Honda, M., and Phillips, D., 2011. High abundances of noble gas and chlorine delivered to the mantle by serpentinite subduction. *Nat. Geosci.* **4**, 807-812.

Kobayashi, M., Sumino, H., Nagao, K., Ishimaru, S., Arai, S., Yoshikawa, M., Kawamoto, T., Kumagai, Y., Kobayashi, T., Burgess, R., and Ballentine, C. J., 2017. Slab-derived halogens and noble gases illuminate closed system processes controlling volatile element transport into the mantle wedge. *Earth and Planetary Science Letters* **457,** 106-116.

Kodolányi, J. and Pettke, T., 2011. Loss of trace elements from serpentinites during fluid-assisted transformation of chrysotile to antigorite - An example from Guatemala. *Chemical Geology* **284**, 351-362.

Kodolányi, J., Pettke, T., Spandler, C., Kamber, B. S., and Gméling, K., 2012. Geochemistry of Ocean Floor and Fore-arc Serpentinites: Constraints on the Ultramafic Input to Subduction Zones. *J. Petrol.* **53**, 235-270.

Kohlstedt, D. L., Keppler, H., and Rubie, D. C., 1996. Solubility of water in the alpha, beta and gamma phases of (Mg,Fe)(2)SiO4. *Contributions to Mineralogy and Petrology* **123**, 345-357.

Lafay, R., Fernandez-Martinez, A., Montes-Hernandez, G., Auzende, A. L., and Poulain, A., 2016. Dissolution-reprecipitation and self-assembly of serpentine nanoparticles preceding chrysotile formation: Insights into the structure of proto-serpentine. *Am. Miner.* **101**, 2666-2676.

López Sanchez-Vizcaino, V., Gomez-Pugnaire, M. T., Garrido, C. J., Padron-Navarta, J. A., and Mellini, M., 2009. Breakdown mechanisms of titanclinohumite in antigorite serpentinite (Cerro del Almirez massif, S. Spain): A petrological and TEM study. *Lithos* **107**, 216-226.

López Sanchez-Vizcaino, V., Trommsdorff, V., Gomez-Pugnaire, M. T., Garrido, C. J., Muntener, O., and Connolly, J. A. D., 2005. Petrology of titanian clinohumite and olivine at the high-pressure breakdown of antigorite serpentinite to chlorite harzburgite (Almirez Massif, S. Spain). *Contributions to Mineralogy and Petrology* **149**, 627-646.

Marchesi, C., Garrido, C. J., Padron-Navarta, J. A., Sanchez-Vizcaino, V. L., and Gomez-Pugnaire, M. T., 2013. Element mobility from seafloor serpentinization to high-pressure dehydration of antigorite in subducted serpentinite: Insights from the Cerro del Almirez ultramafic massif (southern Spain). *Lithos* **178**, 128-142.

Marks, M. A. W., Wenzel, T., Whitehouse, M. J., Loose, M., Zack, T., Barth, M., Worgard, L., Krasz, V., Eby, G. N., Stosnach, H., and Markl, G., 2012. The volatile inventory (F, Cl, Br, S, C) of magmatic apatite: An integrated analytical approach. *Chemical Geology* **291**, 241-255.

Matsuda, J. and Nagao, K., 1986. Noble-Gas Abundances in a Deep-Sea Sediment Core from Eastern Equatorial Pacific. *Geochem. J.* **20**, 71-80.

Michel, A. and Villemant, B., 2003. Determination of halogens (F, Cl, Br, I), sulfur and water in seventeen geological reference materials. Geostandards Newsletter-the Journal of *Geostandards and Geoanalysis* **27**, 163-171.

Moreira, M. and Charnoz, S., 2016. The origin of the neon isotopes in chondrites and on Earth. *Earth and Planetary Science Letters* **433**, 249-256.

Mukhopadhyay, S., 2012. Early differentiation and volatile accretion recorded in deep-mantle neon and xenon. *Nature* **486**, 101-104.

Nadzri, A., Schauries, D., Mota-Santiago, P., Trautmann, C., Gleadow, A. J. W., Hawley, A., and Kluth, P., 2017. Composition and orientation dependent annealing of ion tracks in apatite - Implications for fission track thermochronology. *Chemical Geology* **451**, 9-16.

Nimis, P. and Trommsdorff, V., 2001. Revised thermobarometry of Alpe Arami and other garnet peridotites from the Central Alps. *J. Petrol.* **42**, 103-115.

Ozima, M. and Podosek, F. A., 2002. *Noble Gas Geochemistry*. Cambridge University Press.

Padron-Navarta, J. A., Sanchez-Vizcaino, V. L., Garrido, C. J., and Gomez-Pugnaire, M. T., 2011. Metamorphic Record of High-pressure Dehydration of Antigorite Serpentinite to Chlorite Harzburgite in a Subduction Setting (Cerro del Almirez, Nevado-Filabride Complex, Southern Spain). *J. Petrol.* **52**, 2047-2078.

Padron-Navarta, J. A., Sanchez-Vizcaino, V. L., Hermann, J., Connolly, J. A. D., Garrido, C. J., Gomez-Pugnaire, M. T., and Marchesi, C., 2013. Tschermak's substitution in antigorite and consequences for phase relations and water liberation in high-grade serpentinites. *Lithos* **178**, 186-196.

915 Padron-Navarta, J. A., Tommasi, A., Garrido, C. J., and Mainprice, D., 2015. On topotaxy and
916 compaction during antigorite and chlorite dehydration: an experimental and natural study.
917 *Contributions to Mineralogy and Petrology* **169**.
918 Page, L., Hattori, K., de Hoog, J. C. M., and Okay, A. I., 2016. Halogen (F, Cl, Br, I) behaviour in
919 subducting slabs: A study of lawsonite blueschists in western Turkey. *Earth and Planetary*
920 *Science Letters* **442**, 133-142.
921 Palme, H., O'Neill, H.S.C., 2003. Cosmochemical estimates of Mantle Composition. In: Holland, H.,
922 Turekian, K.K. (Eds.), Treatise on Geochemistry. Elsevier, New York, pp. 1-38.
923 Peters, D., Bretscher, A., John, T., Scambelluri, M., and Pettke, T., 2017. Fluid-mobile elements in
924 serpentinites: Constraints on serpentinisation environments and element cycling in
925 subduction zones. *Chemical Geology* **466**, 654-666.
926 Péron, S., Moreira, M., Colin, A., Arbaret, L., Putlitz, B., and Kurz, M. D., 2016. Neon isotopic
927 composition of the mantle constrained by single vesicle analyses. *Earth and Planetary*
928 *Science Letters* **449**, 145-154.
929 Péron, S., Moreira, M., Putlitz, B., and Kurz, M. D., 2017. Solar wind implantation supplied light
930 volatiles during the first stage of Earth accretion. *Geochemical Perspectives Letters* **3**, 151-
931 159.
932 Philippot, P., Agrinier, P., and Scambelluri, M., 1998. Chlorine cycling during subduction of altered
933 oceanic crust. *Earth and Planetary Science Letters* **161**, 33-44.
934 Pitre, F. and Pinti, D. L., 2010. Noble gas enrichments in porewater of estuarine sediments and their
935 effect on the estimation of net denitrification rates. *Geochimica et Cosmochimica Acta* **74**,
936 531-539.
937 Plumper, O., Royne, A., Magraso, A., and Jamtveit, B., 2012. The interface-scale mechanism of
938 reaction-induced fracturing during serpentinization. *Geology* **40**, 1103-1106.
939 Podosek, F. A., Honda, M., and Ozima, M., 1980. Sedimentary Noble Gases. *Geochimica et*
940 *Cosmochimica Acta* **44**, 1875-1884.
941 Puga, E., Nieto, J. M., de Federico, A. D., Bodinier, J. L., and Morten, L., 1999. Petrology and
942 metamorphic evolution of ultramafic rocks and dolerite dykes of the Betic Ophiolitic
943 Association (Mulhacen Complex, SE Spain): evidence of eo-Alpine subduction following an
944 ocean-floor metasomatic process. *Lithos* **49**, 23-56.
945 Ranero, C. R., Phipps Morgan, J., McIntosh, K., and Reichert, C., 2003. Bending-related faulting and
946 mantle serpentinization at the Middle America trench. *Nature* **425**, 367-373.
947 Raquin, A. and Moreira, M., 2009. Atmospheric Ar-38/Ar-36 in the mantle: Implications for the
948 nature of the terrestrial parent bodies. *Earth and Planetary Science Letters* **287**, 551-558.
949 Risold, A. C., Trommsdorff, V., and Grobety, B., 2001. Genesis of ilmenite rods and palisades along
950 humite-type defects in olivine from Alpe Arami. *Contributions to Mineralogy and Petrology*
951 **140**, 619-628.
952 Roddick, J. C., 1983. High precision intercalibration of 40Ar-39Ar standards. *Geochimica et*
953 *Cosmochimica Acta* **47**, 887-898.
954 Rude, P. D. and Aller, R. C., 1991. Fluorine mobility during early diagenesis of carbonate sediment:
955 An indicator of mineral transformations. *Geochimica et Cosmochimica Acta* **55**, 2491-2509.
956 Scaillet, S., 1996. Excess 40Ar transport scale and mechanism in high-pressure phengites: A case
957 study from an eclogitized metabasite of the Dora-Maira nappe, western Alps. *Geochimica et*
958 *Cosmochimica Acta* **60**, 1075-1090.
959 Scambelluri, M., Bottazzi, P., Trommsdorff, V., Vannucci, R., Hermann, J., Gòmez-Pugnaire, M. T., and
960 Lòpez-Sànchez Vizcaino, V., 2001. Incompatible element-rich fluids released by antigorite
961 breakdown in deeply subducted mantle. *Earth and Planetary Science Letters* **192**, 457-470.
962 Scambelluri, M., Fiebig, J., Malaspina, N., Müntener, O., and Pettke, T., 2004a. Serpentinite
963 Subduction: Implications for Fluid Processes and Trace-Element Recycling. *International*
964 *Geology Review* **46**, 595-613.

965 Scambelluri, M., Müntener, O., Hermann, J., Piccardo, G. B., and Trommsdorff, V., 1995. Subduction
966 of water into the mantle - History of an Alpine Peridotite *Geology* **23**, 459-462.
967 Scambelluri, M., Müntener, O., Ottolini, L., Pettke, T. T., and Vannucci, R., 2004b. The fate of B, Cl
968 and Li in the subducted oceanic mantle and in the antigorite breakdown fluids. *Earth and*
969 *Planetary Science Letters* **222**, 217-234.
970 Scambelluri, M., Pettke, T., and Cannaò, E., 2015. Fluid-related inclusions in Alpine high-pressure
971 peridotite reveal trace element recycling during subduction-zone dehydration of
972 serpentinized mantle (Cima di Gagnone, Swiss Alps). *Earth and Planetary Science Letters* **429**,
973 45-59.
974 Scambelluri, M., Pettke, T., Rampone, E., Godard, M., and Reusser, E., 2014. Petrology and Trace
975 Element Budgets of High-pressure Peridotites Indicate Subduction Dehydration of
976 Serpentinized Mantle (Cima di Gagnone, Central Alps, Switzerland). *J. Petrol.* **55**, 459-498.
977 Scambelluri, M., Piccardo, G. B., Philippot, P., Robbiano, A., and Negretti, L., 1997. High salinity fluid
978 inclusions formed from recycled seawater in deeply subducted alpine serpentinite. *Earth*
979 *and Planetary Science Letters* **148**, 485-499.
980 Schmidt, M. W. and Poli, S., 1998. Experimentally based water budgets for dehydrating slabs and
981 consequences for arc magma generation. *Earth and Planetary Science Letters* **163**, 361-379.
982 Seyfried, W. E. and Ding, K., 1995. The hydrothermal chemistry of fluoride in seawater. *Geochimica*
983 *et Cosmochimica Acta* **59**, 1063-1071.
984 Sharp, Z. D. and Barnes, J. D., 2004. Water-soluble chlorides in massive seafloor serpentinites: a
985 source of chloride in subduction zones. *Earth and Planetary Science Letters* **226**, 243-254.
986 Sherlock, S. and Kelley, S., 2002. Excess argon evolution in HP-LT rocks: a UVLAMP study of phengite
987 and K-free minerals, NW Turkey. *Chemical Geology* **182**, 619-636.
988 Sumino, H., Burgess, R., Mizukami, T., Wallis, S. R., Holland, G., and Ballentine, C. J., 2010. Seawater-
989 derived noble gases and halogens preserved in exhumed mantle wedge peridotite. *Earth and*
990 *Planetary Science Letters* **294**, 163-172.
991 Sun, W. D., Binns, R. A., Fan, A. C., Kamenetsky, V. S., Wysoczanski, R., Wei, G. J., Hu, Y. H., and
992 Arculus, R. J., 2007. Chlorine in submarine volcanic glasses from the eastern Manus basin.
993 *Geochimica Et Cosmochimica Acta* **71**, 1542-1552.
994 Trieloff, M., Kunz, J., Clague, D. A., Harrison, D., and Allegre, C. J., 2000. The nature of pristine noble
995 gases in mantle plumes. *Science* **288**, 1036-1038.
996 Trommsdorff, V., Sanchez-Vizcaino, V. L., Gomez-Pugnaire, M. T., and Muntener, O., 1998. High
997 pressure breakdown of antigorite to spinifex-textured olivine and orthopyroxene, SE Spain.
998 *Contributions to Mineralogy and Petrology* **132**, 139-148.
999 Tucker, J. M. and Mukhopadhyay, S., 2014. Evidence for multiple magma ocean outgassing and
1000 atmospheric loss episodes from mantle noble gases. *Earth and Planetary Science Letters* **393,**
1001 254-265.
1002 Workman, R.K., Hart, S.R., 2005. Major and trace element composition of the depleted MORB
1003 mantle (DMM). *Earth and Planetary Science Letters*, **231**(1-2): 53-72.
1004 Yokochi, R. and Marty, B., 2004. A determination of the neon isotopic composition of the deep
1005 mantle. *Earth and Planetary Science Letters* **225**, 77-88.
1006

Table 1. Summary of atmospheric and irradiation-produced Ar isotope release in low temperature heating steps

	Chrysotile serpentinites		Antigorite serpentinites		Chlorite harzburgites		Garnet peridotites	
	^{36}Ar	$^{38}Ar_{Cl}$	^{36}Ar	$^{38}Ar_{Cl}$	^{36}Ar	$^{38}Ar_{Cl}$	^{36}Ar	$^{38}Ar_{Cl}$
range	17-95%	4-46%	5-84%	6-18%	9-33%	5-16%	10-54%	1%
Average	47%	18%	57%	13%	28%	18%	29%	1%
$\%^{36}Ar/\%^{38}Ar_{Cl}$	3.7		4.5		2.5		25	

Irradiated samples were analysed in two heating steps: the data here show the proportion of gas released in the low temperature steps at 300 or 400 °C.

Table 2. Halogens in serpentinites and their metamorphosed equivalents

	CaO Wt.%	K ppm	Cl ppm	Br ppb	I ppb	F ppm	Br/Cl $\times10^{-3}$	I/Cl $\times10^{-6}$
	Noble gas method on mineral separates					SIMS		
Chrysotile serpentinites								
Seafloor (n = 9)[1]	0.3-8.5	4-74	500-1700	1300-6800	17-500	<20	2.7-5.6	28-290
Fore-arc (n = 8)[1]	0.2-0.8	13-270	400-2300	2700-23,000	2000-45,000		5.3-10.4	2000-43,000
Erro Tobbio (n = 3)[1]	0.5-3.4	<37	330-740	1300-3400	490-1330	<20	3.8-4.6	870-1900
Antigorite serpentinites								
Erro Tobbio (n = 5)[2]	0.3-7.1	8-63	75-570	260-2100	41-180	<20	2.4-4.1	170-790
Cerro del Almirez								
Alm94	0.52	12	220	200	27	~20	0.92	120
Alm119	0.36	7	250	370	32	<20	1.5	130
Alm125	nd	23	160	270	17	<20	1.7	100
Chlorite harzburgites								
Cerro del Almirez								
Spin. rocks (n = 2)[2]	0.0-0.2	7-130	95-380	130-810	4-72	36-170	1.0-2.1	48-190
Chl-rich veins (n = 2)[2]	0.0-1.1	9-29	67-360	66-310	5-25	180-270	0.7-1.0	52-79
Al08-16 ol/opx –a	0.06	19	170	220	27	16 ± 11	1.3	160
Al08-16 ol/opx –b	0.07	17	200	220	29		1.1	150
Al08-16 chl –a	0.06	20	150	140	43	240 ± 30	0.90	290
Al08-16 chl –b	0.07	18	150	130	42		0.87	290
Al08-16 chl –c	0.13	24	150	140	47		0.93	310
Al08-16 WR	0.09*	18*	180*	210*	30*	49	1.2*	170*
Al10-06 ol/px –a	0.07	12	240	370	26		1.6	110
Al10-06 ol/px –b	0.07	11	210	340	22		1.6	100
Al10-06 chl –a	0.07	8	140	200	44		1.5	330
Al10-06 chl –b	0.08	6	140	170	42		1.2	300
Al10-06 WR	0.07*	11*	150*	210*	27*	78	1.4*	180*
Cima di Gagnone								
Mg31 09-03	0.18	4	36	315	7	39	8.6	210
Garnet peridotite, Cima di Gagnone								
Mg160 - gnt	4.1	7	78	360	14	5 ± 1	4.6	170
Mg160 - ol-opx	0.25	nd	20	100	8	13 ± 2	5.2	380
Mg160 - cpx	19.8	160	290	980	33	10 ± 5	3.3	110
Mg160 – WR	3-4*		~60*	~250*	~12*	~11*	~4.1*	~200*
Mg160 - Peak	3-4*		~40*	~170*	~10*	~10*	~4.8*	~270*
Reference values								
Seawater	0.040	0.038	19,300	66,000	58	1.3	3.5	3.5
Mantle[3]	3.2	40-80	5 ± 2	13 ± 6	0.3 ± 0.1	12 ± 2	2.8 ± 0.8	60 ± 30
Primitive mantle[3]	3.7 ± 0.6	260 ± 80	26 ± 8	76 ± 25	7 ± 4	17 ± 6	2.9 ± 0.6	270 ±120

Analyses are 'total fusion' values based on the total gas released in all heating steps (e.g. 300/400 + 1500 °C).

[1]Data ranges summarised from Kendrick et al. (2013).

[2]Data ranges summarised from Kendrick et al. (2011).

[3]Reference values from (Kendrick et al., 2017; Palme and O'Neill, 2003; Workman and Hart, 2005).

**estimated: Mg160 – WR is estimated based on the model mineralogy (65(Ol+opx):25 (gnt): 10 (cpx + hbl)), whereas the cpx mineral separate is not included in Mg160 – Peak (65(Ol+opx):25 (gnt))*

Table 3. Representative electron microprobe analyses of amphiboles in sample Mg160 (Fig 5)

	Hbl 1	Hbl 3	Hbl 8	Hbl 14	Hbl 15	Hbl 18	Hbl 19	Hbl 20
SiO_2	47.5	46.0	45.7	47.1	47.0	45.8	47.1	47.3
TiO_2	0.48	0.30	0.23	0.47	0.46	0.29	0.42	0.31
Al_2O_3	11.3	13.5	14.1	11.7	11.3	12.7	11.9	11.23
Cr_2O_3	0.59	0.81	0.63	1.4	1.5	1.6	1.5	1.4
FeO*	3.5	3.7	3.7	2.9	3.4	3.3	3.3	3.0
MnO	0.08	0.05	0.08	0.03	0.04	0.05	0.05	0.07
MgO	19.0	18.1	17.8	18.9	19.4	18.5	19.1	19.3
CaO	11.9	12.5	12.4	12.5	11.8	12.5	12.2	12.7
Na_2O	2.8	3.2	3.4	2.9	3.0	2.8	2.8	2.6
K_2O	0.37	0.11	0.05	0.16	0.13	0.45	0.08	0.52
Total	96.6**	97.5	97.4	97.2	97.1	97.5	97.4	97.7
Cl ppm	730	3190	5870	1650	740	3450	560	2660

**Total Fe reported as FeO. **low total a result of sample charging. All amphiboles contain ~2 wt % H_2O. Amphibole (Hbl) numbers correspond to amphiboles identified in Figure 5.*

Table 4. Noble gases in irradiated serpentinites and their metamorphosed equivalents

	Mass mg	^{36}Ar mol/g $\times10^{-15}$	^{84}Kr/^{36}Ar	^{130}Xe/^{36}Ar	^{40}Ar/^{36}Ar
Chrysotile serpentinites					
Seafloor (n = 9)[1]		80-5,400	0.026-0.056	0.00030-0.00124	303-380
Fore-arc (n = 8)[1]		200-3,400	0.029-0.044	0.00046-0.00106	307-342
Erro Tobbio (n = 3)[1]		550-1400	0.025-0.030	0.00023-0.00033	320-322
Antigorite serpentinites					
Erro Tobbio (n = 5)[2]		210-740	0.03-0.05	0.0004-0.0011	310-390
Cerro del Almirez					
Alm94	27.3	750	0.049 ± 0.004	0.00079 ± 0.00008	321 ± 4
Alm119	27.3	330	0.049 ± 0.004	0.00068 ± 0.00008	375 ± 10
Alm125	27.5	430	0.037 ± 0.003	0.00035 ± 0.00005	390 ± 23
Chlorite harzburgites					
Cerro del Almirez					
Spin. rocks (n = 2)[2]		23-260	0.06-0.10	0.0016-0.0041	360-600
Chl.-rich veins (n =2)[2]		21-220	0.05-0.08	0.0009-0.0018	375-700
Al08-16 ol –a	34.4	70	0.054 ± 0.010	0.00187 ± 0.00038	379 ± 59
Al08-16 ol –b	28.1	9.4	0.045 ± 0.036	0.00209 ± 0.00205	690 ± 530
Al08-16 chl –a	20.7	470	0.028 ± 0.003	0.00064 ± 0.00009	311 ± 23
Al08-16 chl –b	23	640	0.028 ± 0.003	0.00053 ± 0.00003	297 ± 7
Al08-16 chl –c	14.6	320	0.028 ± 0.004	0.00079 ± 0.00015	299 ± 33
Al10-06 ol –a	37.0	66	0.039 ± 0.011	0.00103 ± 0.00032	380 ± 100
Al10-06 ol –b	36.8	78	0.042 ± 0.012	0.00117 ± 0.00038	371 ± 95
Al10-06 chl –a	21.0	220	0.036 ± 0.005	0.00126 ± 0.00018	294 ± 26
Al10-06 chl –b	28.6	210	0.037 ± 0.005	0.00124 ± 0.00015	305 ± 21
Cima di Gagnone					
Mg31 09-03	32.6	290	0.033 ± 0.003	0.00052 ± 0.00007	349 ± 24
Garnet peridotite, Cima di Gagnone					
Mg160 - gnt	45.1	46	0.044 ± 0.005	0.00096 ± 0.00033	1080 ± 270
Mg160 - olv-opx	42.8	25	0.046 ± 0.026	0.00200 ± 0.00117	720 ± 400
Mg160 - cpx	56.2	120	0.045 ± 0.006	0.00074 ± 0.00014	1160 ± 90
Mg160 – WR		~40*	~0.045*	~0.001*	~1000*
Mg160 - Peak		~31*	~0.045*	~0.001*	~900*

Analyses are based on the high temperature heating step only (e.g. 1500 or 1600 °C). Uncertainties are 2σ.

[1]*Data ranges summarised from Kendrick et al. (2013).*

[2]*Data ranges summarised from Kendrick et al. (2011).*

Table 5. Noble gases in non-irradiated serpentinites and their metamorphosed equivalents

	Mass mg	^{36}Ar mol/g $\times 10^{-15}$	^{4}He/^{36}Ar	^{20}Ne/^{36}Ar	^{84}Kr/^{36}Ar	^{130}Xe/^{36}Ar	^{40}Ar/^{36}Ar
Chrysotile serpentinites							
Seafloor (n = 4)[1]		110-630	2.1-109	0.02-0.10	nd	nd	296-317
Fore-arc (n = 2)[1]		500-630	0.2-0.9	0.13-0.19	nd	nd	~296
Antigorite serpentinites							
Erro Tobbio (n = 3)[2]		90-590	nd	0.06-0.10	0.029-0.044	0.00056-0.0015	308-332
Cerro del Almirez							
Alm94	97.5	65	2760 ± 220	0.11 ± 0.10	0.0019 ± 0.0002	0.00087 ± 0.00008	372 ± 10
Alm125	97.3	130	1800 ± 140	0.22 ± 0.04	0.0024 ± 0.0002	0.00036 ± 0.00004	509 ± 6
Chlorite harzburgites							
Cerro del Almirez							
Spin. rocks (n = 2)[2]		18-108	nd	0.075-0.53	0.028-0.063	0.00032-0.0033	370-633
Veins (n = 2)[2]		43-119		0.18-0.32	0.039-0.055	0.00060-0.0013	373-536
Al08-16 ol	203	66	2120 ± 370	0.17 ± 0.05	0.079 ± 0.009	0.00071 ± 0.00017	488 ± 4
Al08-16 chl	110	230	800 ± 80	0.29 ± 0.05	0.020 ± 0.002	0.00147 ± 0.00016	308 ± 18
Al10-06 WR	215	130	2370 ± 190	0.11 ± 0.03	0.036 ± 0.003	0.00559 ± 0.00053	340 ± 2
Cima di Gagnone							
Mg31 09-03	199	180	550 ± 100	0.29 ± 0.04	0.027 ± 0.003	0.00073 ± 0.00010	646 ± 2
Garnet peridotite, Cima di Gagnone							
Mg160-WR	538	56	1160 ± 90	0.21 ± 0.04	nd	0.00077 ± 0.00012	935 ± 5
Reference values							
Atmosphere		-	0.17	0.52	0.021	0.00011	296
Seawater 25 °C		34,000	0.05	0.17	0.036	0.00035	296
Mantle		~2	3000-7000	~1.4	~0.06	~0.001	~10,000-30,000

Analyses are based on total fusion in a single heating step at 1500 or 1600 °C. Uncertainties are 2σ.

[1]*Data ranges summarised from Kendrick et al. (2013).*

[2]*Data ranges summarised from Kendrick et al. (2011).*

[3]*Reference values from Ozima and Podosek (2002).*

Fig 1 (Kendrick et al., 2017)

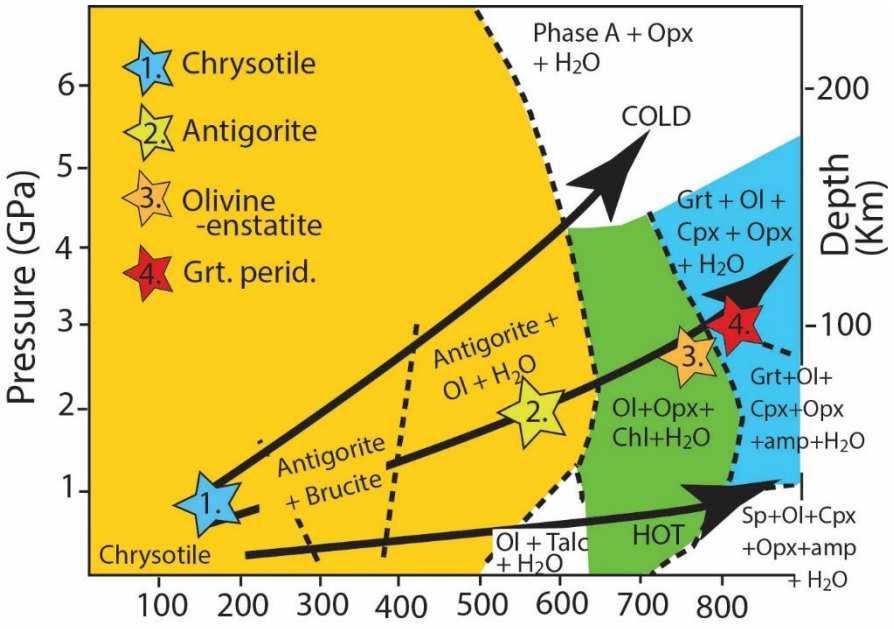

Fig 1. Schematic phase diagram showing the relationships between mineral phases in seafloor serpentinites and their metamorphosed equivalents. The diagram is modified from Scambelluri et al. (2004) and (2014). Note that the exact positions of phase boundaries and mineral assemblages (e.g. presence of amphibole) vary with composition, see pseudosections in Scambelluri et al. (2014).

Fig 2 (Kendrick et al., 2017)

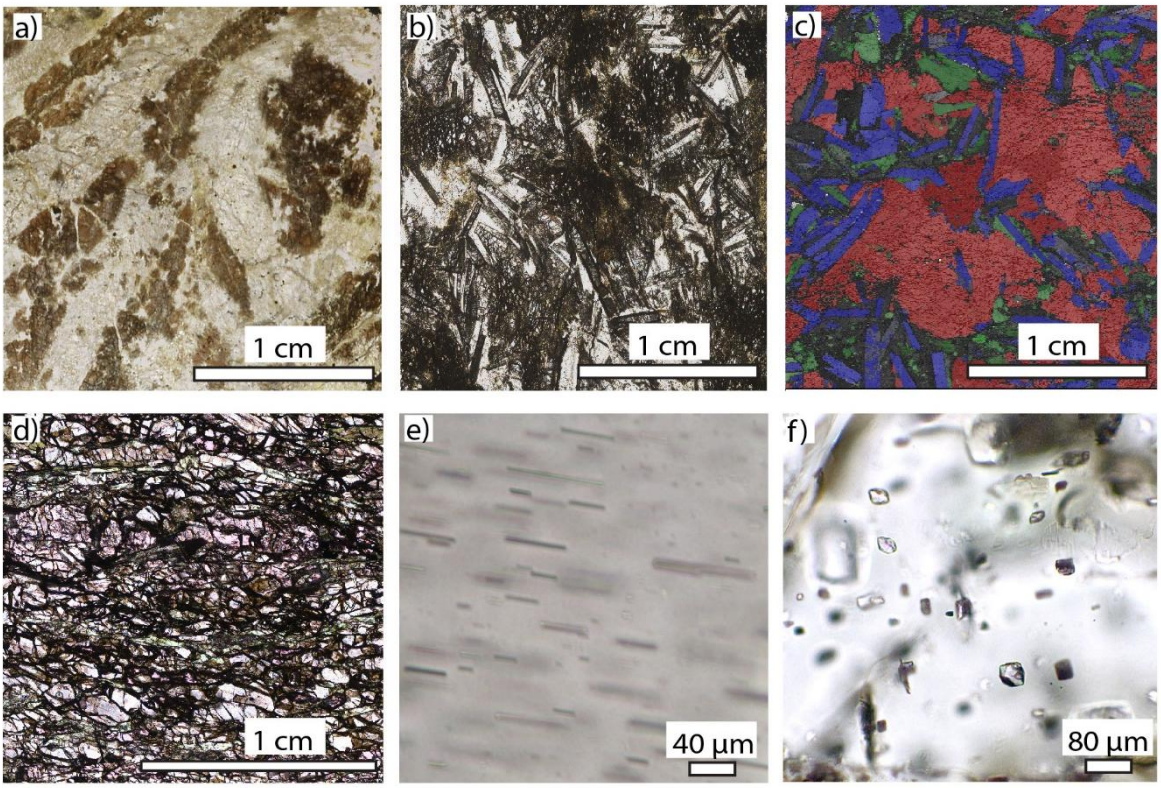

Fig 2. Photomicrographs of representative peridotite sample materials. A) Alm 8 is an example of a spinifex textured chlorite harzburgite in which brown spinifex olivine is in an enstatite dominated matrix. B) AL10-06 is a granofels chlorite harzburgite with abundant chlorite clots, c) shows a phase map of the same sample (blue =,enstatite, red = olivine, green = chlorite). d) Garnet peridotite Mg160. e) close up of ilmenite needles in olivine of sample Mg160. f) a representative example of desiccated fluid inclusion remnants in a sample from Mg160, similar fluid inclusion remnants are found in nominally anhydrous minerals in all of the secondary peridotites investigated.

Fig 3 (Kendrick et al., 2017)

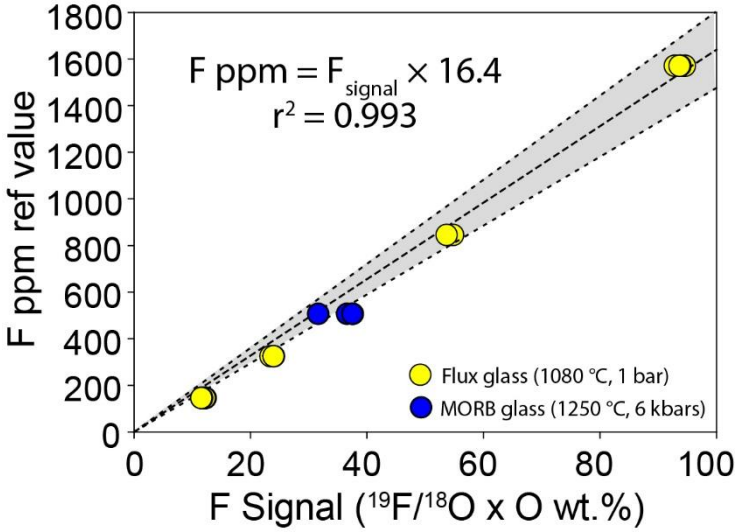

Fig 3. The calibration curve used to determine F concentrations from SHRIMP-II data. The curve is based on the repeat analyses of CaF_2 doped flux glasses analysed at regular intervals during a 48 hr analytical session. The least squares regression is forced through the origin and a 10% error envelope is shown. A F-doped synthetic MORB glass was prepared in a piston cylinder and lies on the same curve.

Fig 4 (Kendrick et al., 2017)

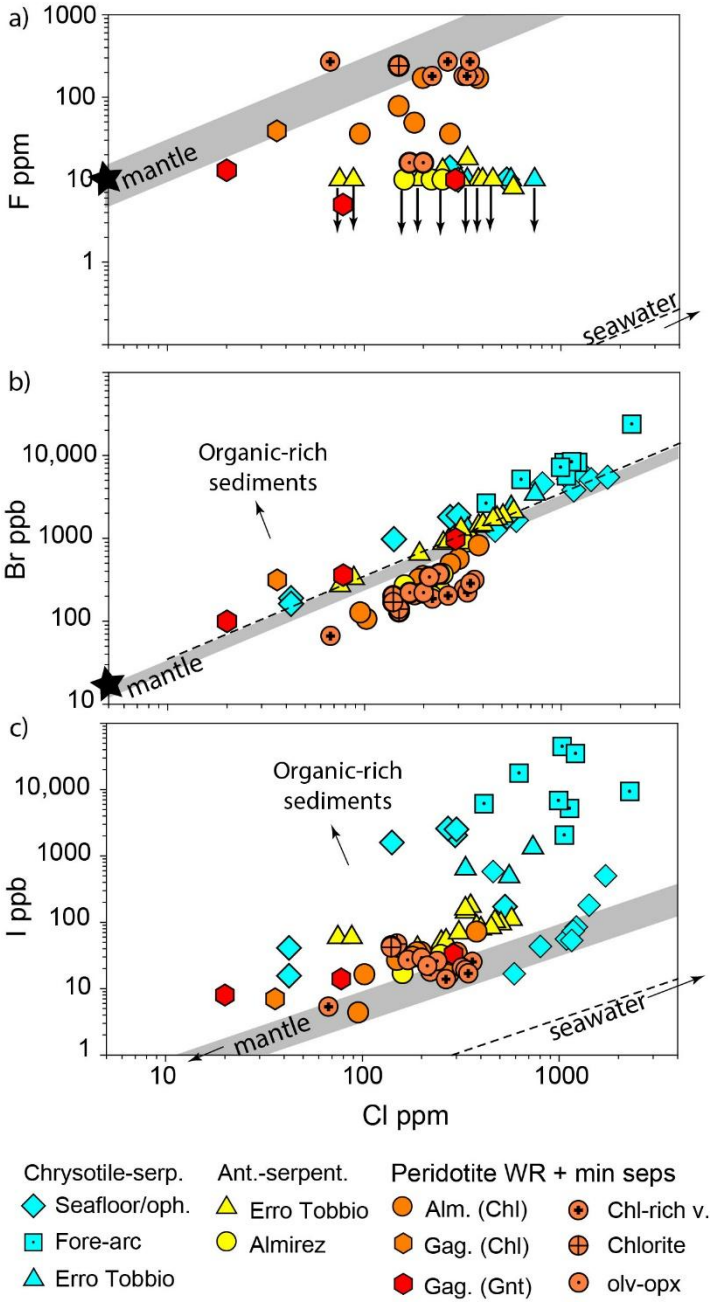

Fig 4. Halogen concentrations in serpentinites, their metamorphosed equivalents and mineral separates. The average concentrations of F, Cl and Br in the depleted mantle (Kendrick et al., 2017) is shown by the black stars in a and b and the F/Cl, Br/Cl and I/Cl ratios of the mantle and seawater are shown by the sloping grey fields and dashed lines in panel a, b and c, respectively.

Fig 5 (Kendrick et al., 2017)

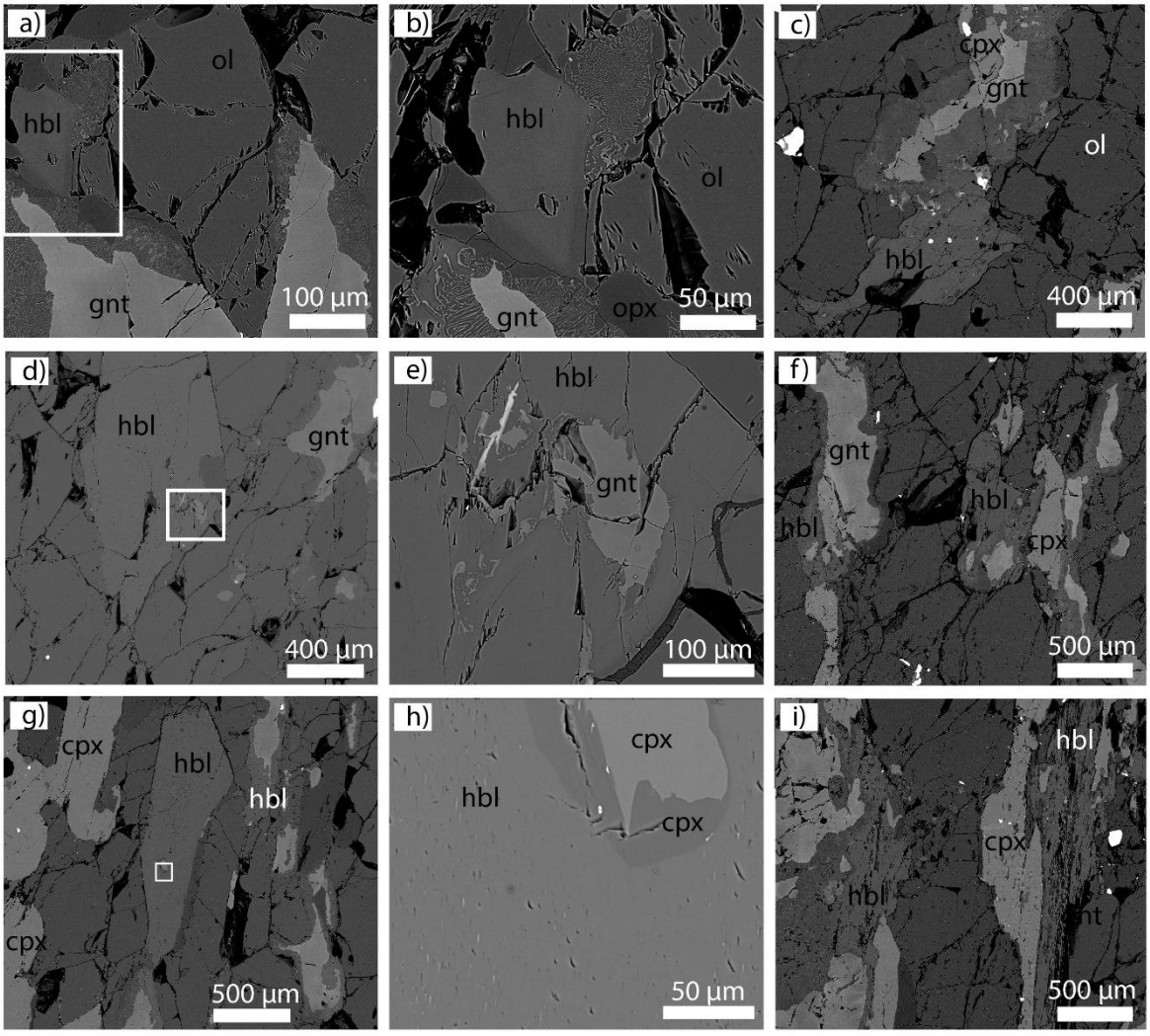

Fig 5. Backscattered electron images of amphibole in sample Mg160. a,b) show hornblende (amp3) closely associated with kelyphite rims on garnet. Note that the garnet has completely reacted away from the symplectite in the upper part of b. c) a larger kelyphite rim, which is larger than the remaining garnet core (amp18). d) a mm-sized hbl with inclusion of garnet (amp14). e) the close up of the inclusion shows a replacement texture. f) hornblende associated with garnet and cpx (amp19). g) another example of a mm sized amphibole, the cpx inclusion boxed is shown in part h (amp15). h) the cpx inclusion has been eroded by replacement and has a dark reaction rim. Brightly coloured lamellae are visible in the hornblende, providing further evidence for its replacive origin. i) elongated hornblende adjacent to cpx (amp20) and between garnet and cpx on the left.

Fig 6 (Kendrick et al., 2017)

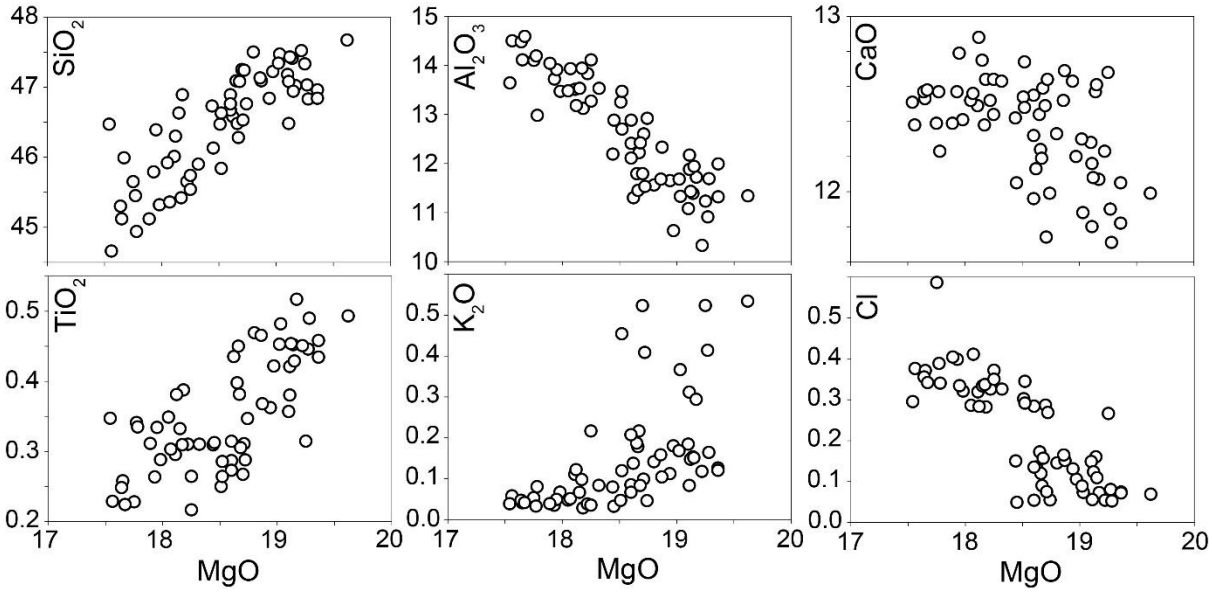

Fig 6. Electron microprobe data (wt %) for amphiboles in Mg160. Representative examples are shown in Fig 5. All amphiboles are loosely described as Mg-rich hornblendes. Cl is roughly correlated with major elements such as Mg, Si and Al, and minor elements like Ti, but it is not correlated with K.

Fig 7 (Kendrick et al., 2017)

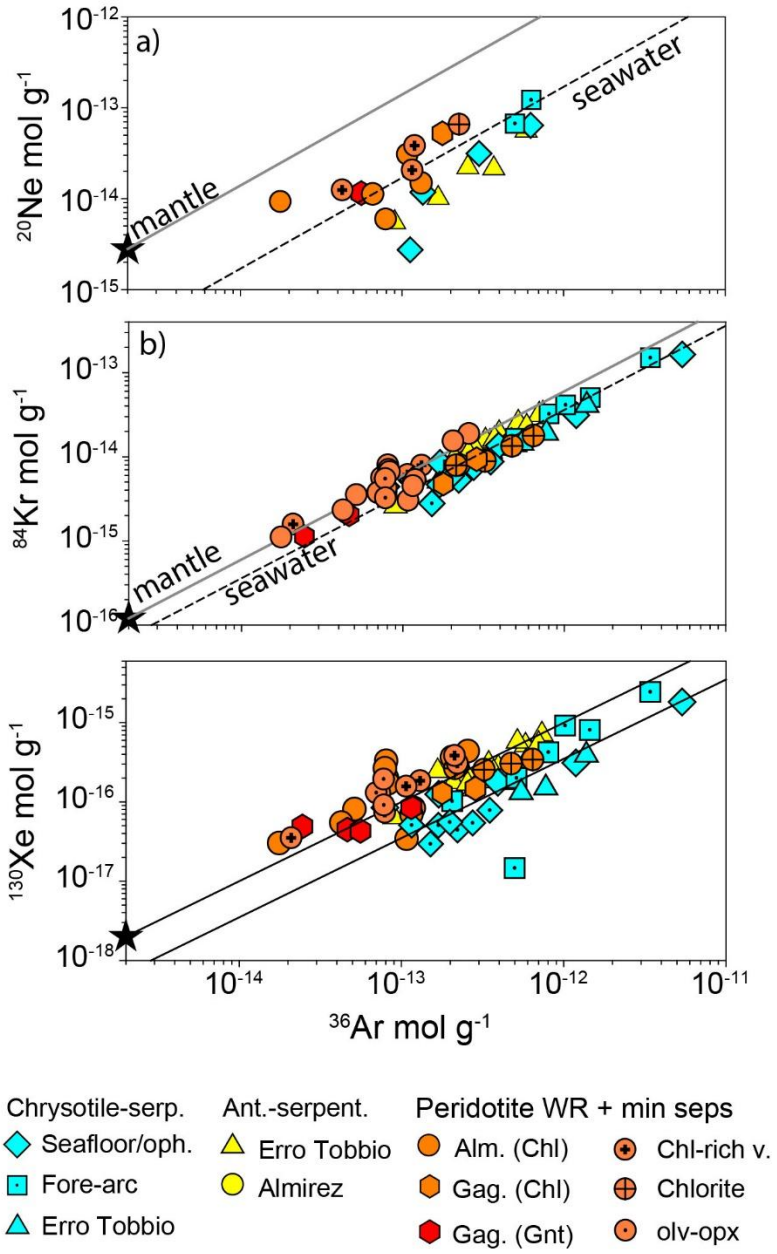

Fig 7. Noble gas concentrations in serpentinites, related rocks and mineral separates. Note that the mantle concentrations of ^{36}Ar, ^{20}Ne, ^{84}Kr and ^{130}Xe estimated by Holland and Ballentine (2006) and slopes representing the ^{20}Ne/^{36}Ar, ^{84}Kr/^{36}Ar and ^{130}Xe/^{36}Ar ratios of the mantle and seawater are shown in parts a, b and c, respectively. Data are from this study (Tables 5 and 6) and Kendrick et al.(2011; 2013).

Fig 8 (Kendrick et al., 2017)

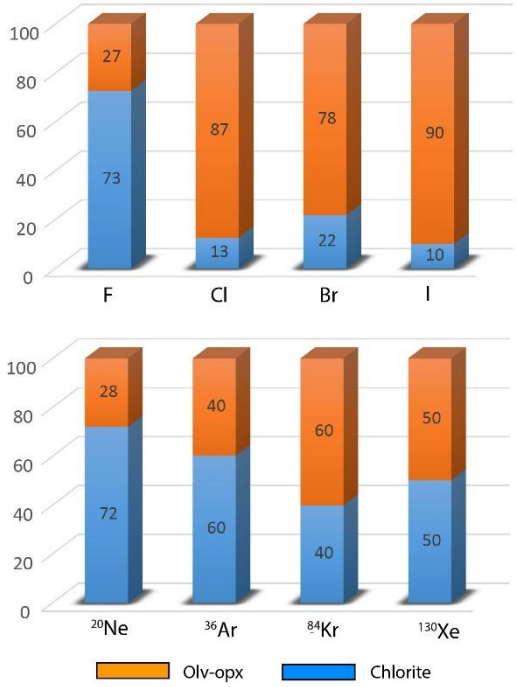

Fig 8. Stacked bar chart showing the distribution of halogens and atmospheric noble gases between the mineral chlorite, which does not host visible fluid inclusions, and olivine-enstatite, which hosts abundant desiccated fluid inclusions (Fig 2f) in the chlorite harzburgite sample Al08-16, which is assumed to have a modal abundance of 15% chlorite. Data are from Tables 2, 5 and 6.

Fig 9 (Kendrick et al., 2017)

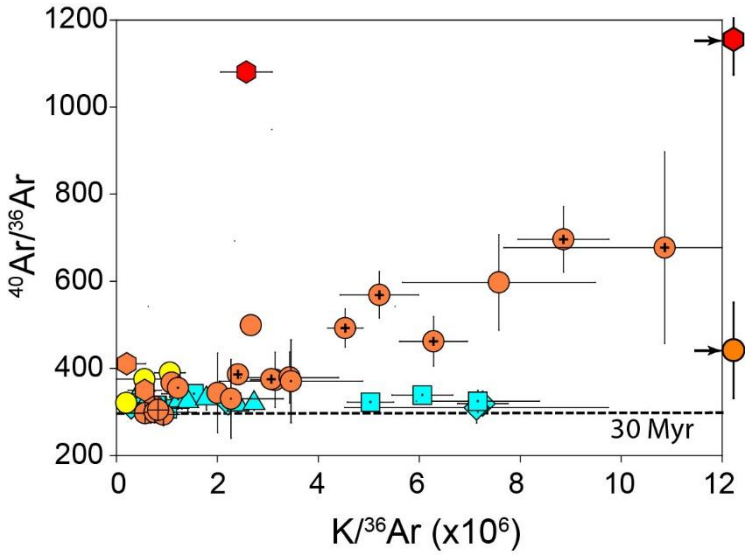

Fig 9. Isochron plot for samples with measurable K. The slope of a 30 Myr isochron is shown as a dotted line for reference and appears almost flat at this scale. All samples are dominated by atmospheric and excess ^{40}Ar, with in situ production of ^{40}Ar being insignificant.

Fig 10 (Kendrick et al., 2017)

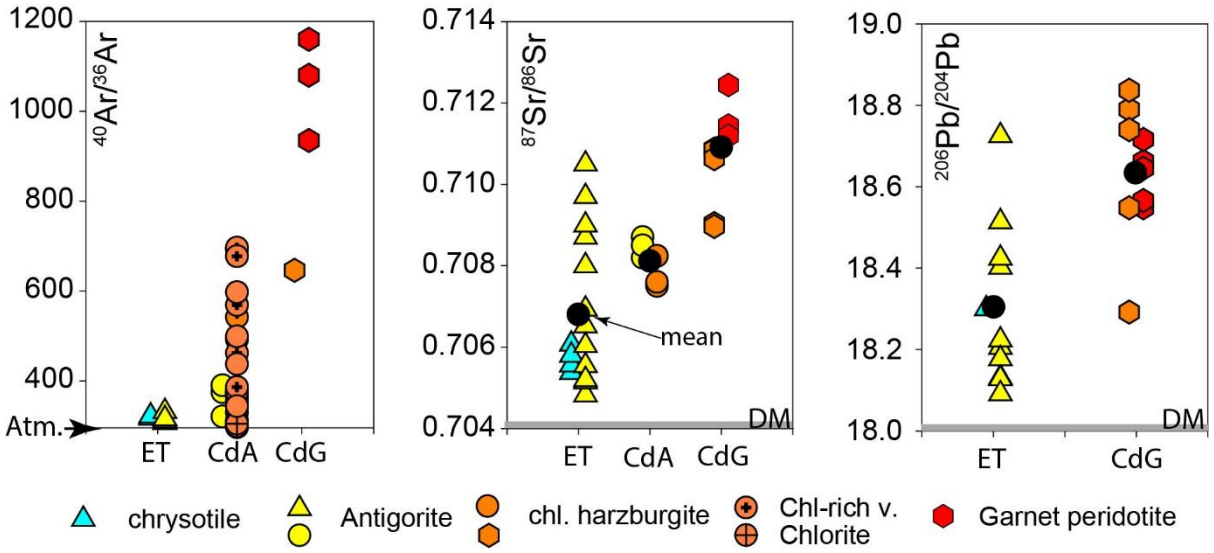

Fig 10. The $^{40}Ar/^{36}Ar$ of serpentinites and related rocks from Erro Tobbio (ET), Cerro del Almirez (CdA) and Cima di Gagnone (CdG) together with previously published $^{87}Sr/^{86}Sr$ and $^{206}Pb/^{204}Pb$ data (Cannaò et al., 2015; 2016; Harvey et al., 2014). The black circles indicate the mean $^{87}Sr/^{86}Sr$ and $^{206}Pb/^{204}Pb$ ratios for each locality. Note that all ophiolite samples are enriched in radiogenic ^{40}Ar relative to seawater and ^{87}Sr and ^{206}Pb compared to the depleted mantle (DM).

Fig 11 (Kendrick et al., 2017)

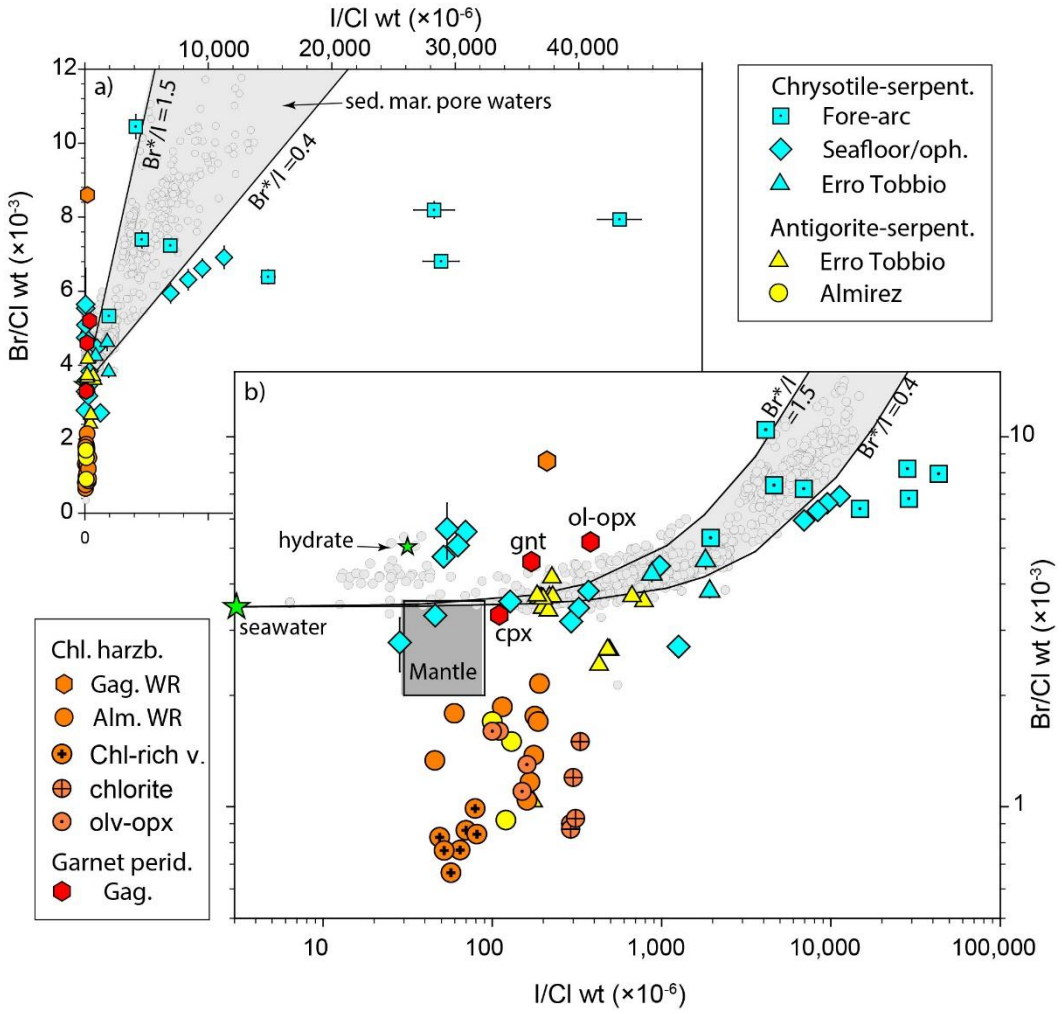

Fig 11. The Br/Cl and I/Cl composition of serpentinites and their metamorphosed equivalents. The data are shown in both linear space (a) and log-log (b) space.

Fig 12 (Kendrick et al., 2017)

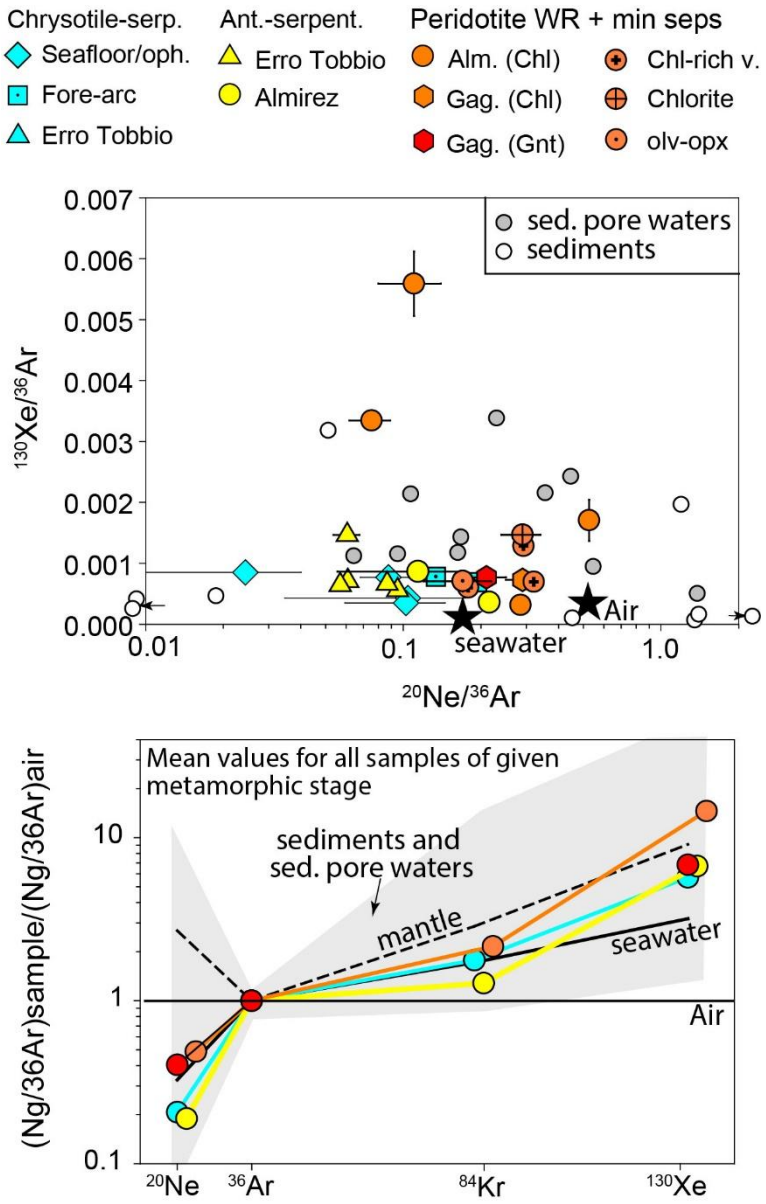

Fig 12. Noble gas abundance ratios for serpentinites and their metamorphosed equivalents. A) $^{20}Ne/^{36}Ar$ versus $^{130}Xe/^{36}Ar$. B) Noble gas fractionation values [$(Ng/^{36}Ar)$ normalised to air] are shown for the four principal lithologies investigated: i) chrysotile serpentinites, ii) antigorite serpentinites, iii) chlorite harzburgites, iv) garnet peridotite. The composition of sedimentary pore waters (Pitre and Pinti, 2010), sediments (Matsuda and Nagoa, 1986; Podosek et al., 1980), seawater, the mantle and air are shown for reference (Ozima and Podosek, 2002).

Fig 13 (Kendrick et al., 2017)

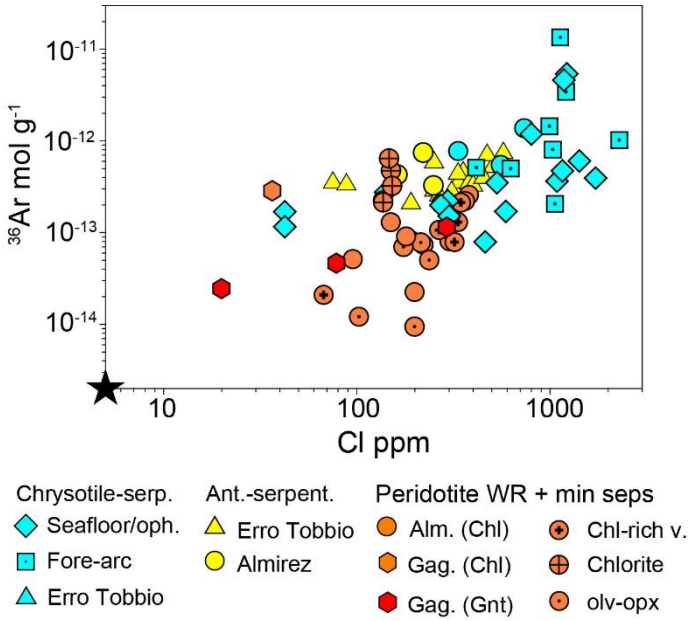

Fig 13. The concentration of Cl versus ^{36}Ar in serpentinites and their dehydrated equivalents. Noble gas and halogen concentrations decrease with increasing metamorphic grade; however, olivine-opx separates obtained from garnet peridotite, retain concentrations several times to an order of magnitude greater than the depleted mantle. Depleted mantle Cl and ^{36}Ar concentrations are from (Holland and Ballentine, 2006; Kendrick et al., 2017).

Fig 14 (Kendrick et al., 2017)

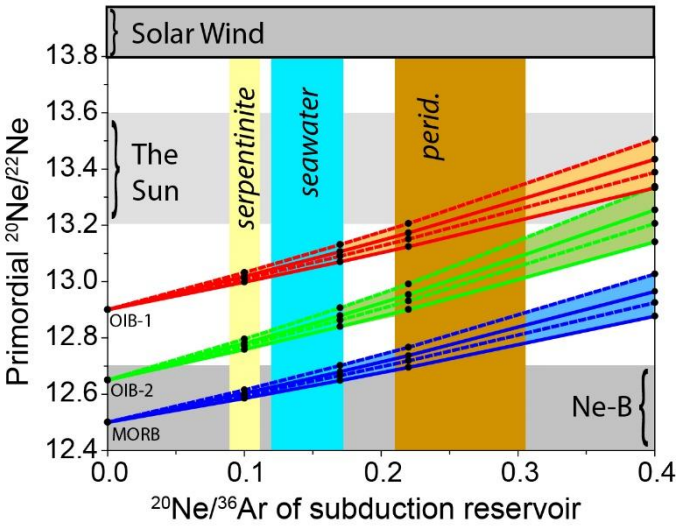

Fig 14. Plot showing how the mantle's $^{20}Ne/^{22}Ne$ ratio could have been modified by subduction of reservoirs with different $^{20}Ne/^{36}Ar$: the reservoirs shown are Ne-poor seafloor serpentinite, seawater with temperature dependent $^{20}Ne/^{36}Ar$ and Ne-enriched peridotites generated by subduction zone processes and dehydration of serpentinites (Fig 10). Possible primordial reservoirs including Ne-B and the Sun are shown as horizontal bands. The curves show that for any reasonable subduction reservoir with realistic $^{20}Ne/^{36}Ar$, the mantle's current $^{20}Ne/^{22}Ne$ must be lower than the primordial value. The mantle reservoirs modelled are OIB-1: $^{20}Ne/^{22}Ne$ = 12.9, $^{22}Ne/^{36}Ar$ =0.25-0.3; OIB-2: $^{20}Ne/^{22}Ne$ = 12.65, $^{22}Ne/^{36}Ar$ =0.21-0.25 and MORB: $^{20}Ne/^{22}Ne$ = 12.5, $^{22}Ne/^{36}Ar$ =0.11-0.16. The dotted lines assume 100% of ^{36}Ar has a subducted origin and the solid lines assume 90% of ^{36}Ar has a subducted origin.

Figure
Click here to download high resolution image

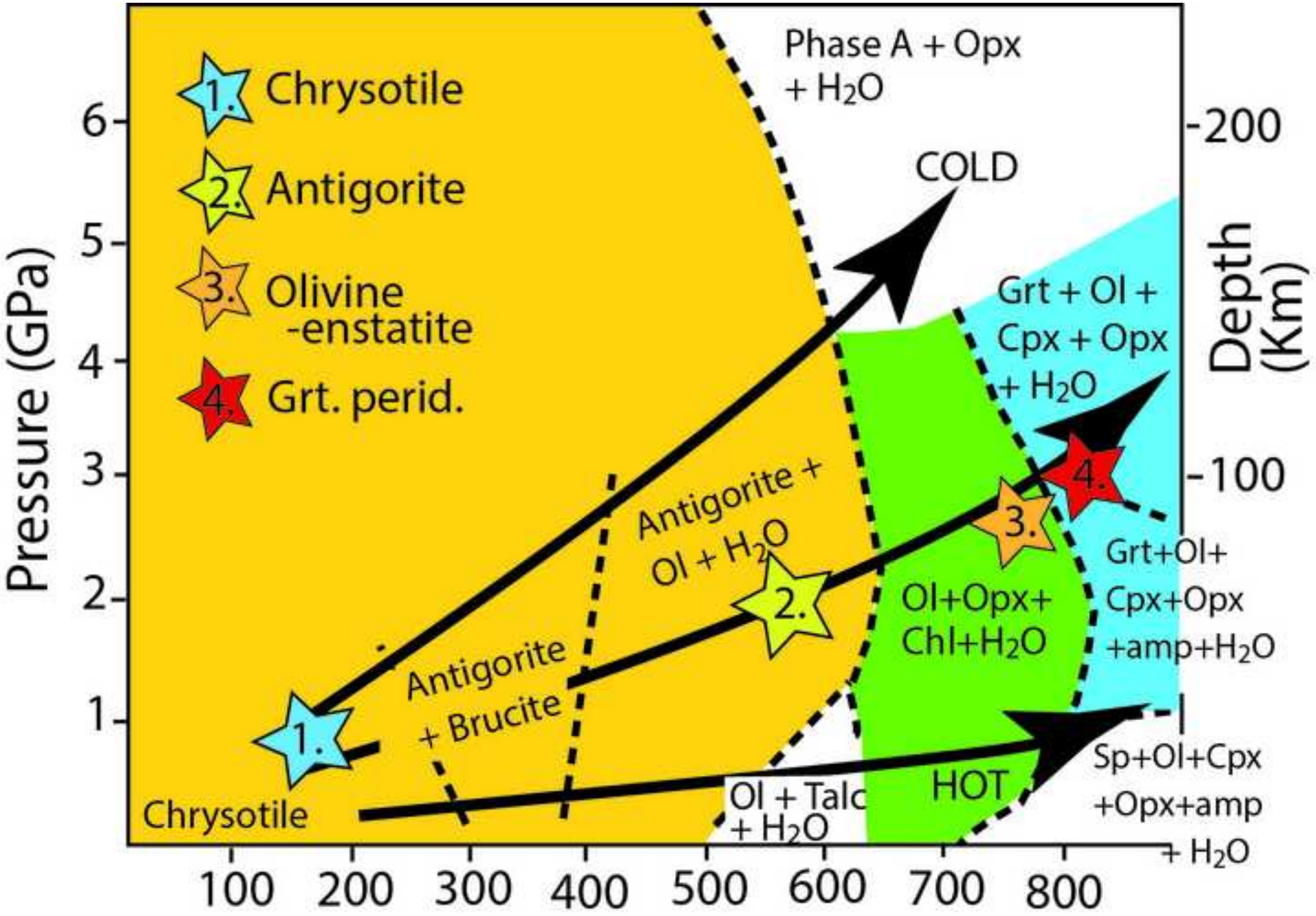

Figure
Click here to download high resolution image

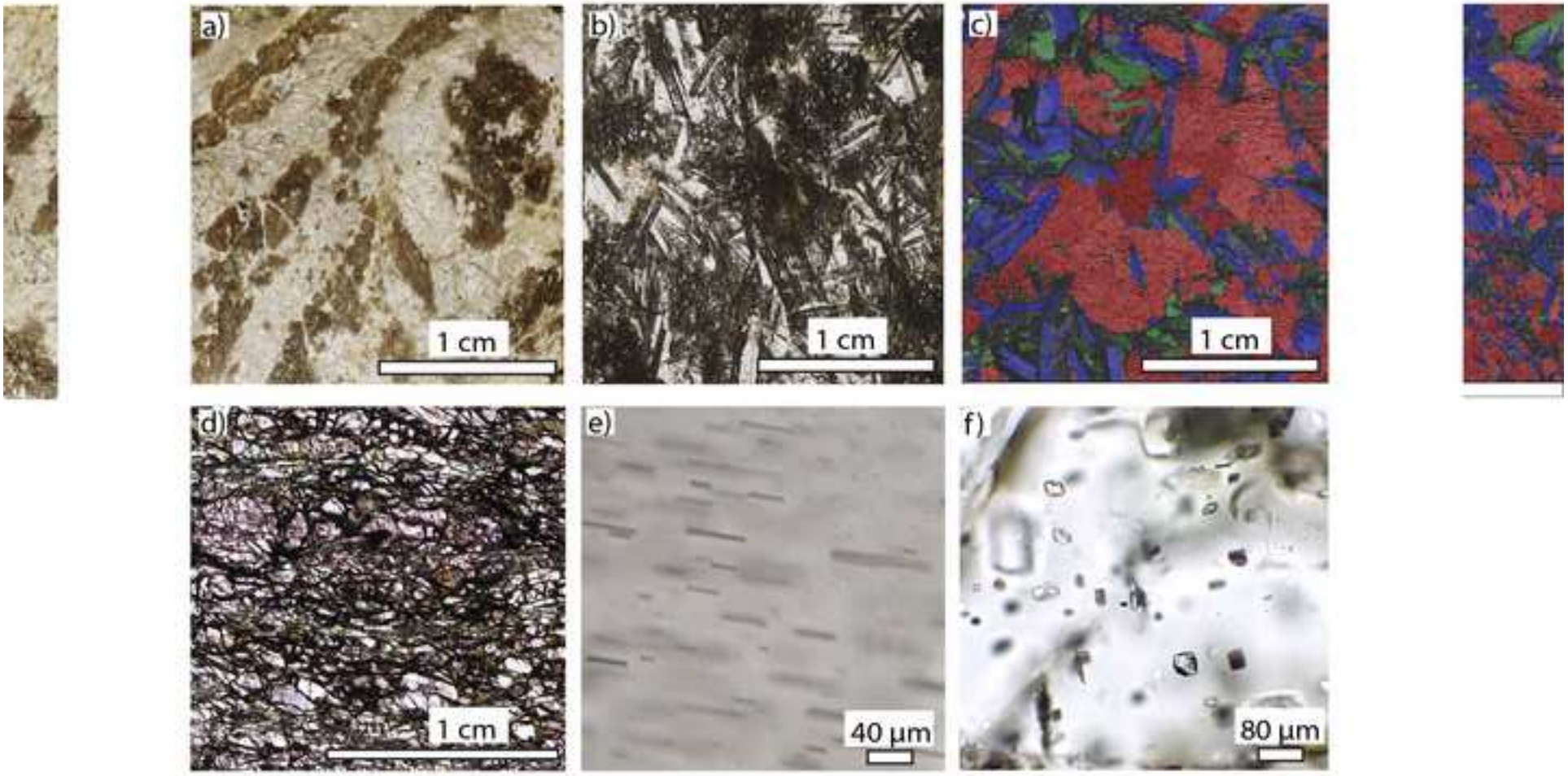

Figure

Click here to download high resolution image

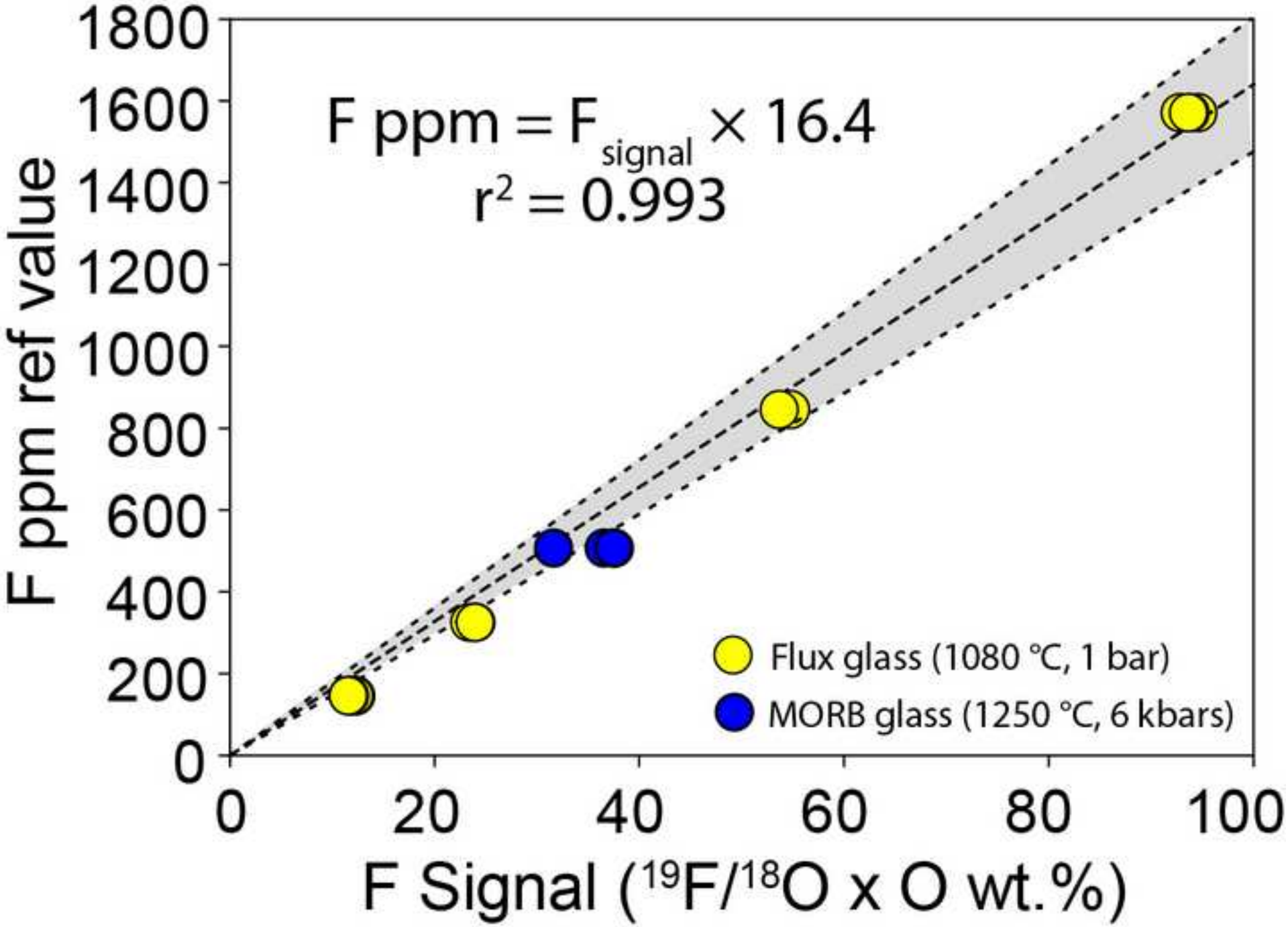

Figure

Click here to download high resolution image

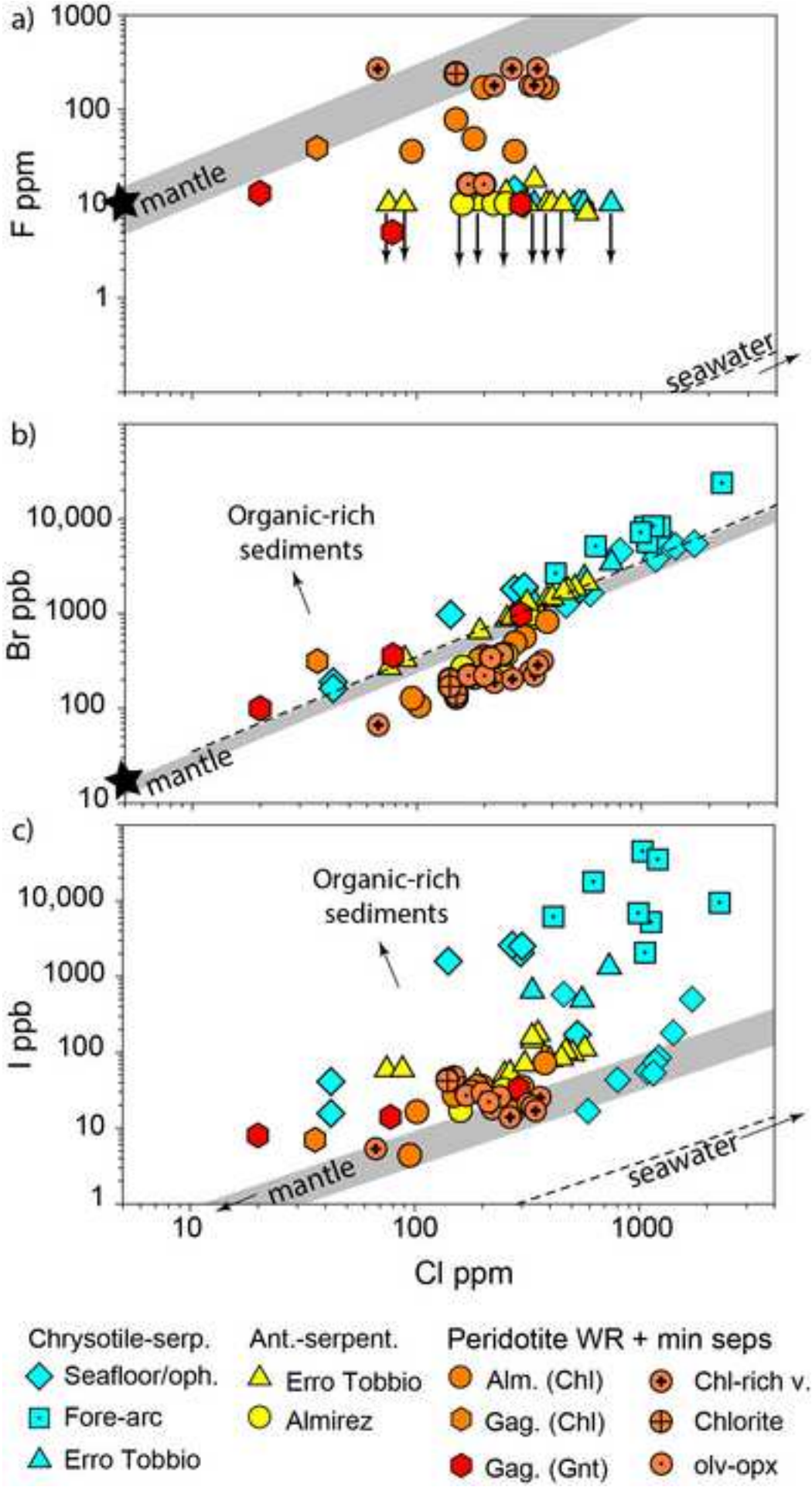

Figure

Click here to download high resolution image

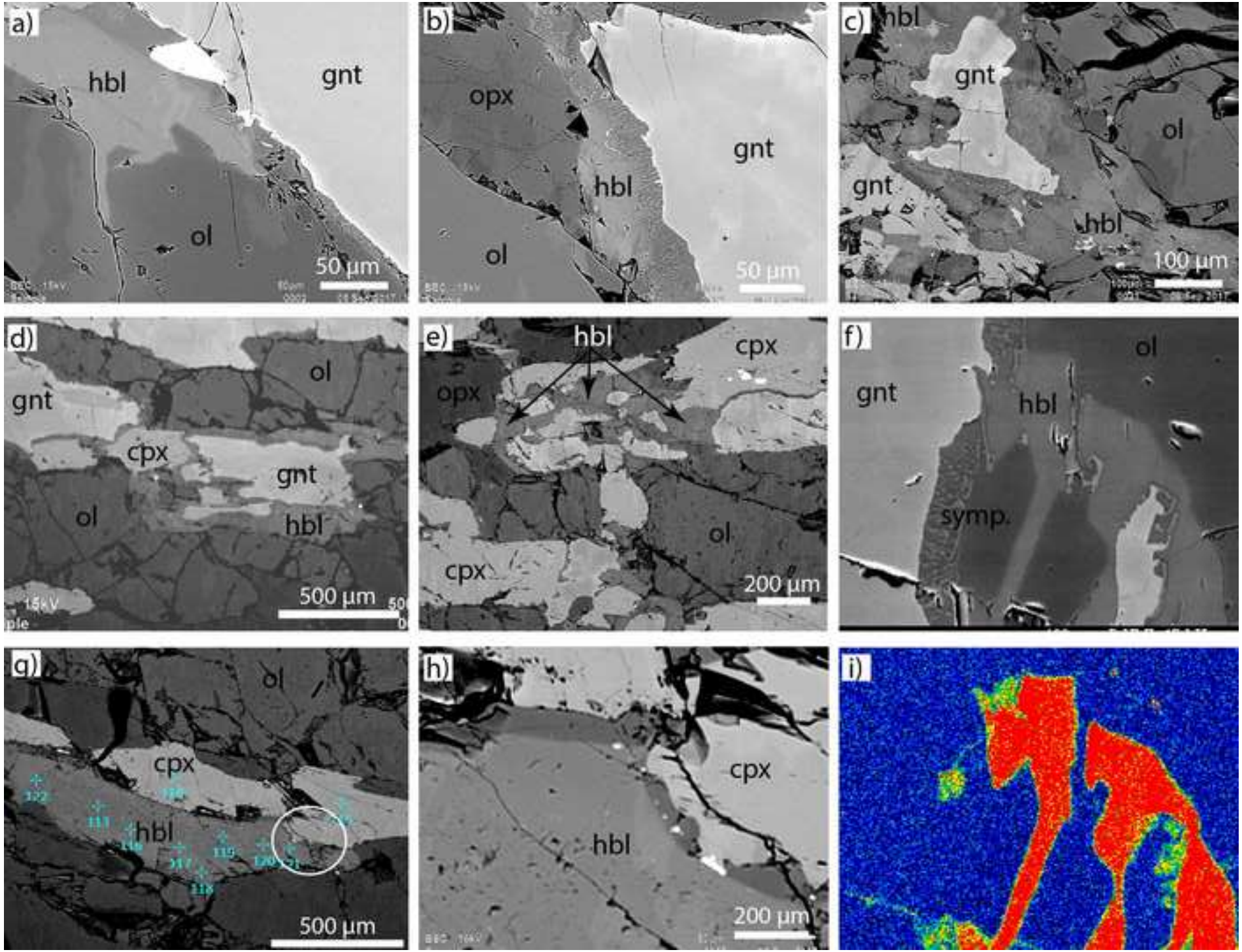

Figure

Click here to download high resolution image

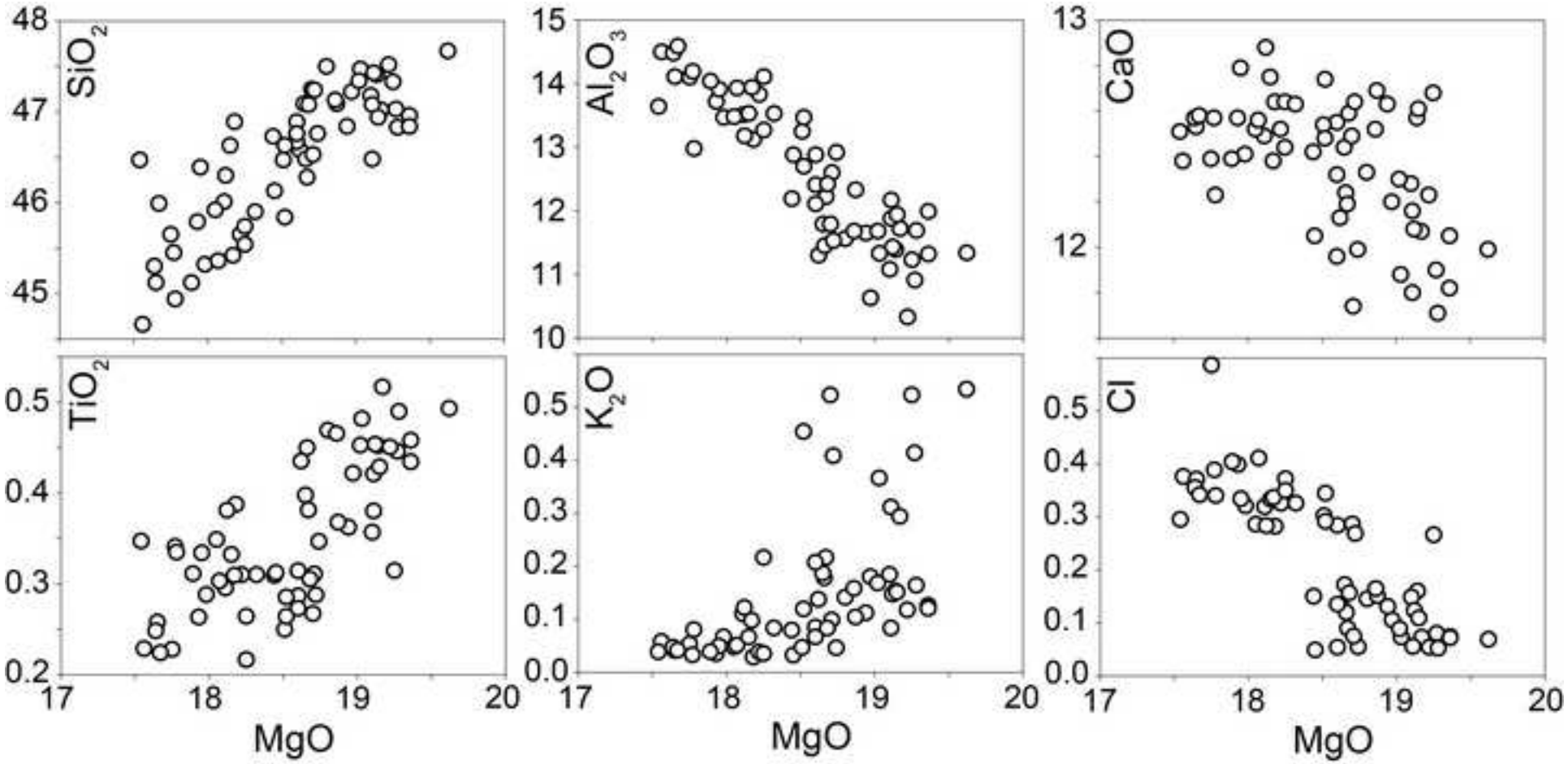

Figure

Click here to download high resolution image

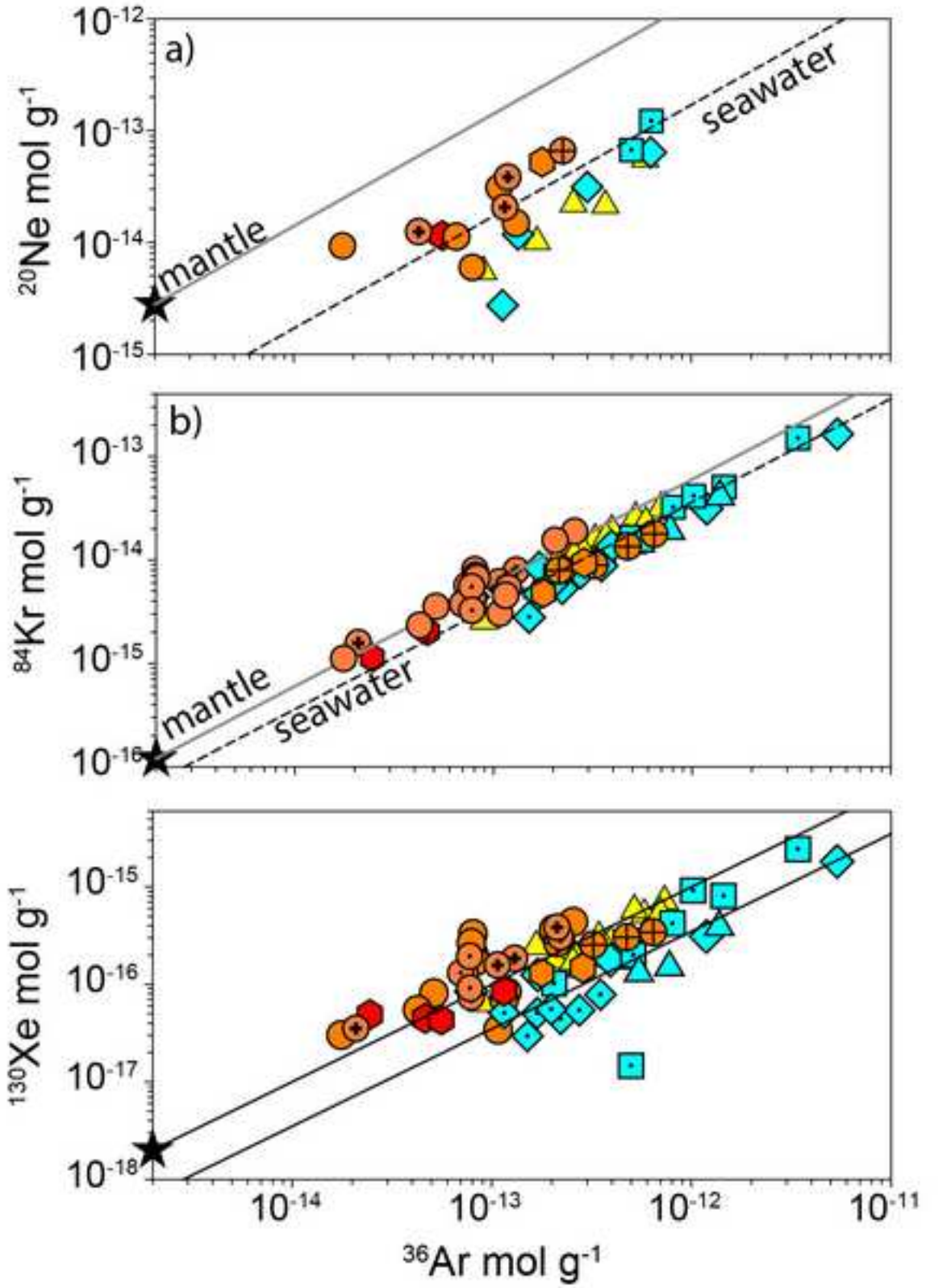

Figure

Click here to download high resolution image

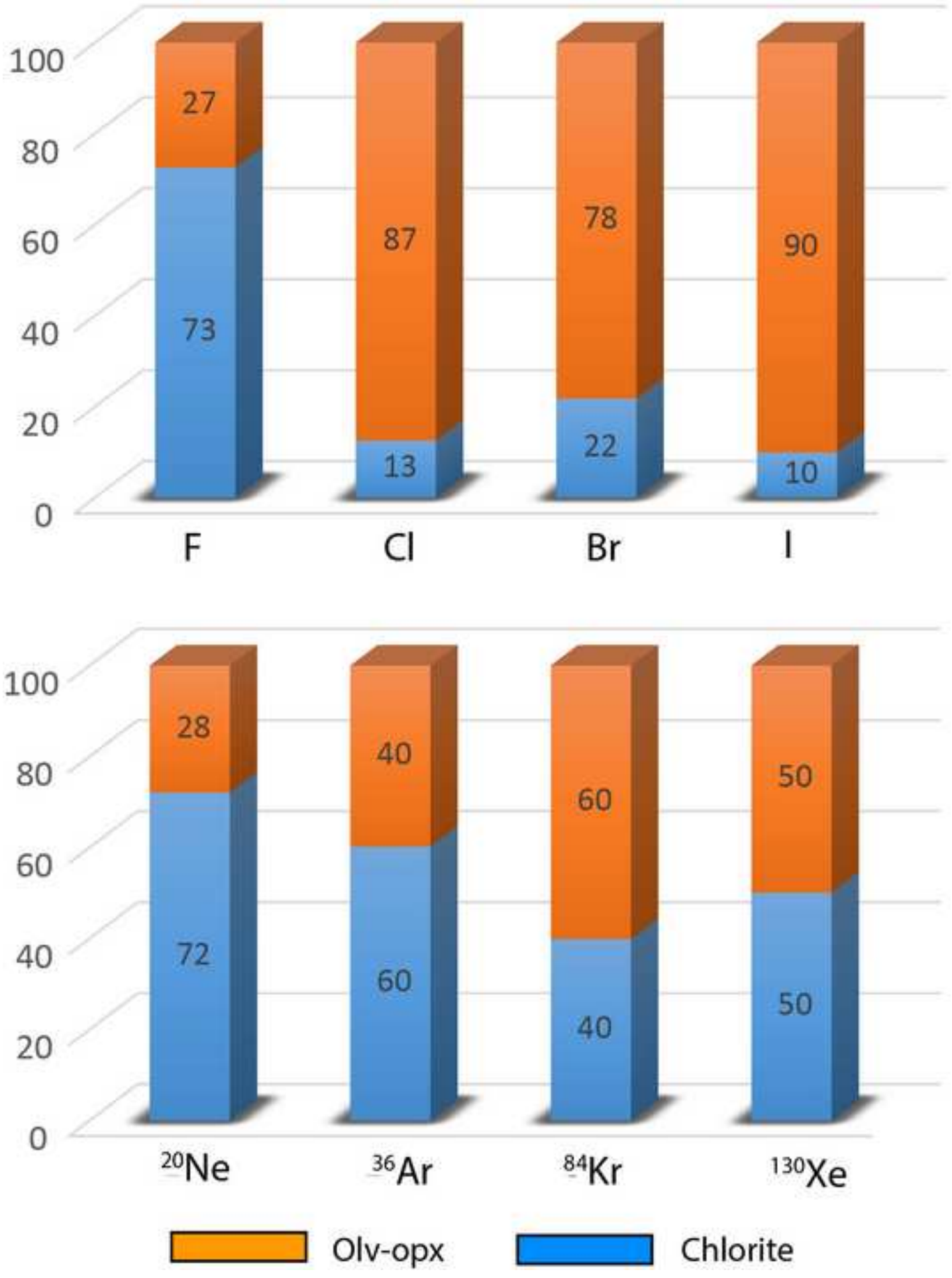

Figure
Click here to download high resolution image

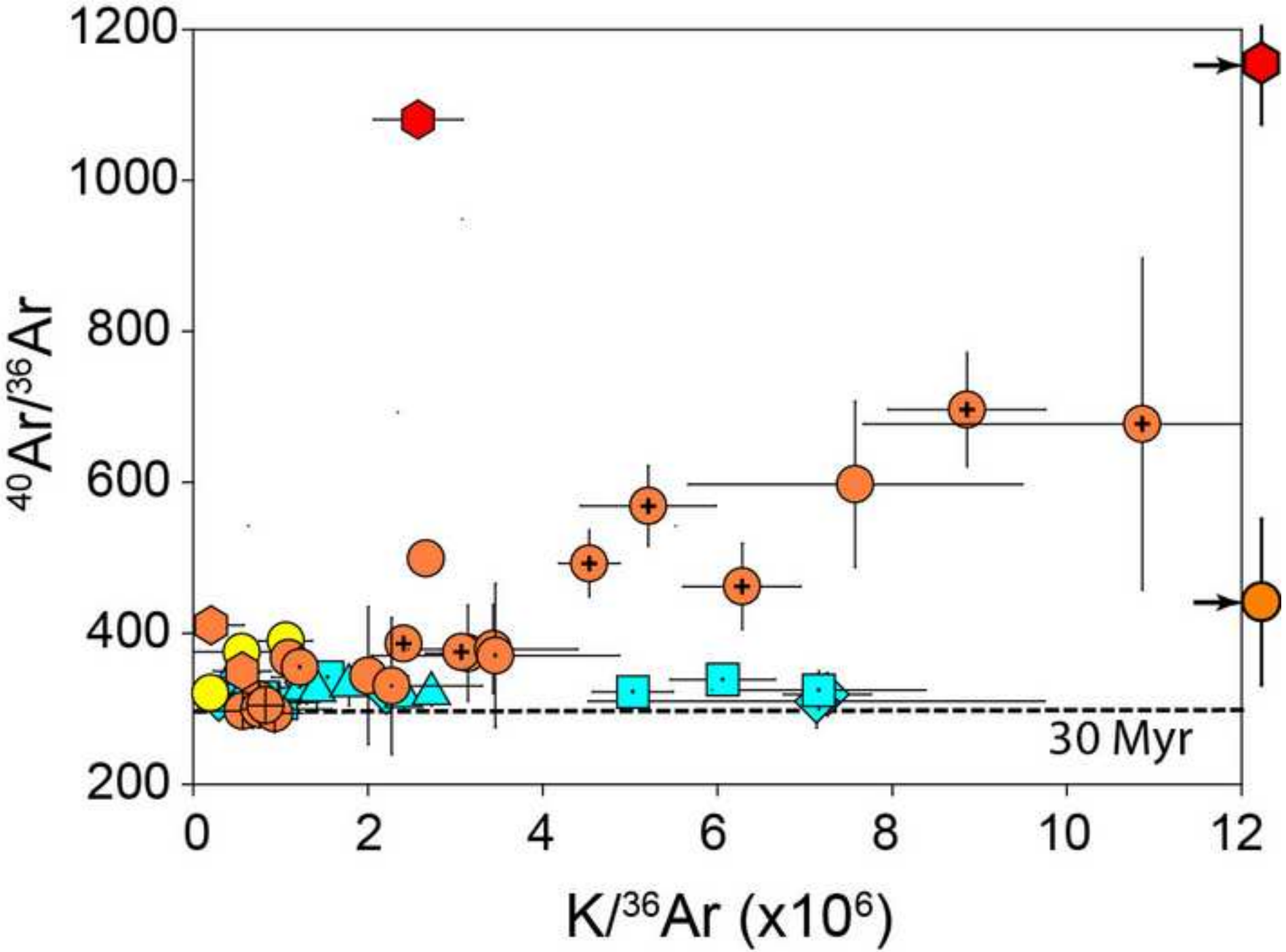

Figure
Click here to download high resolution image

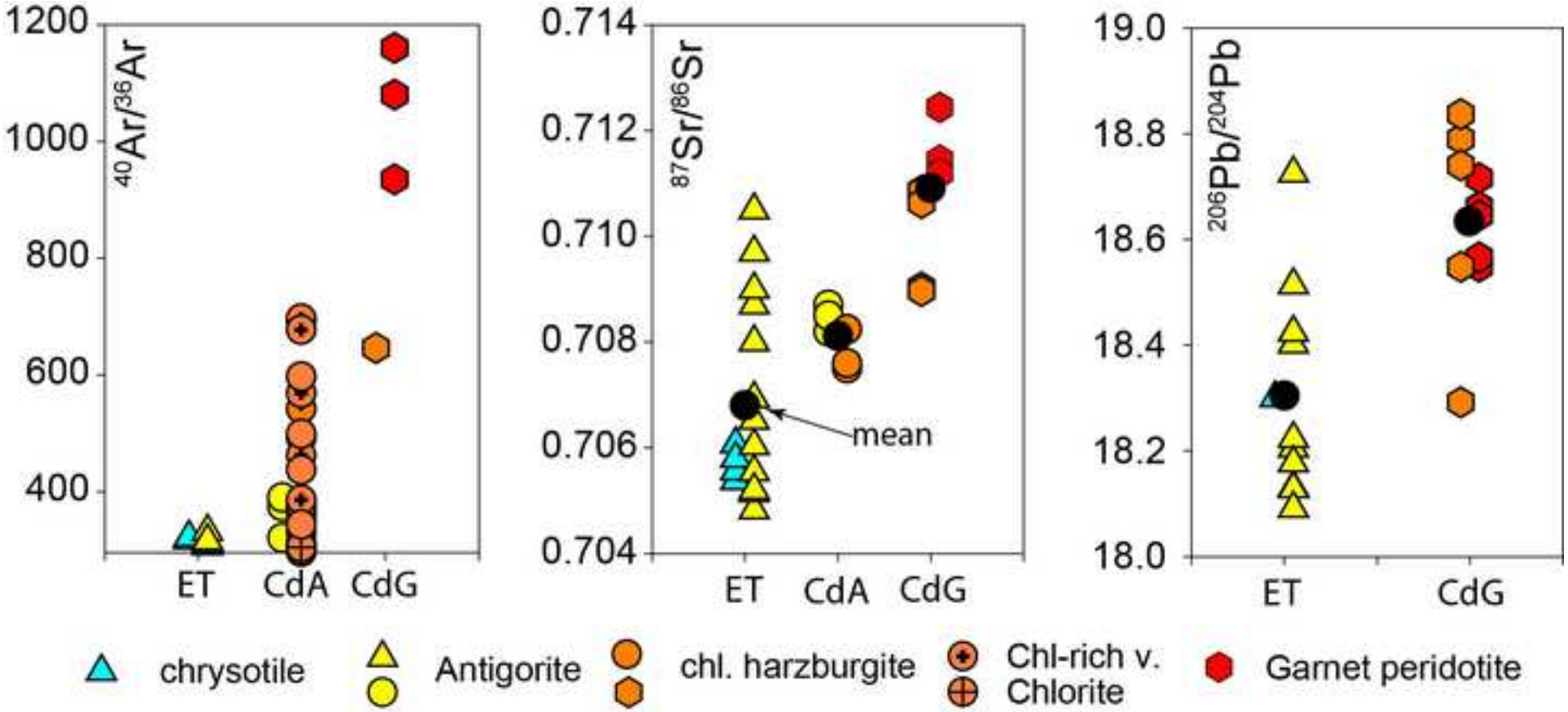

Figure

Click here to download high resolution image

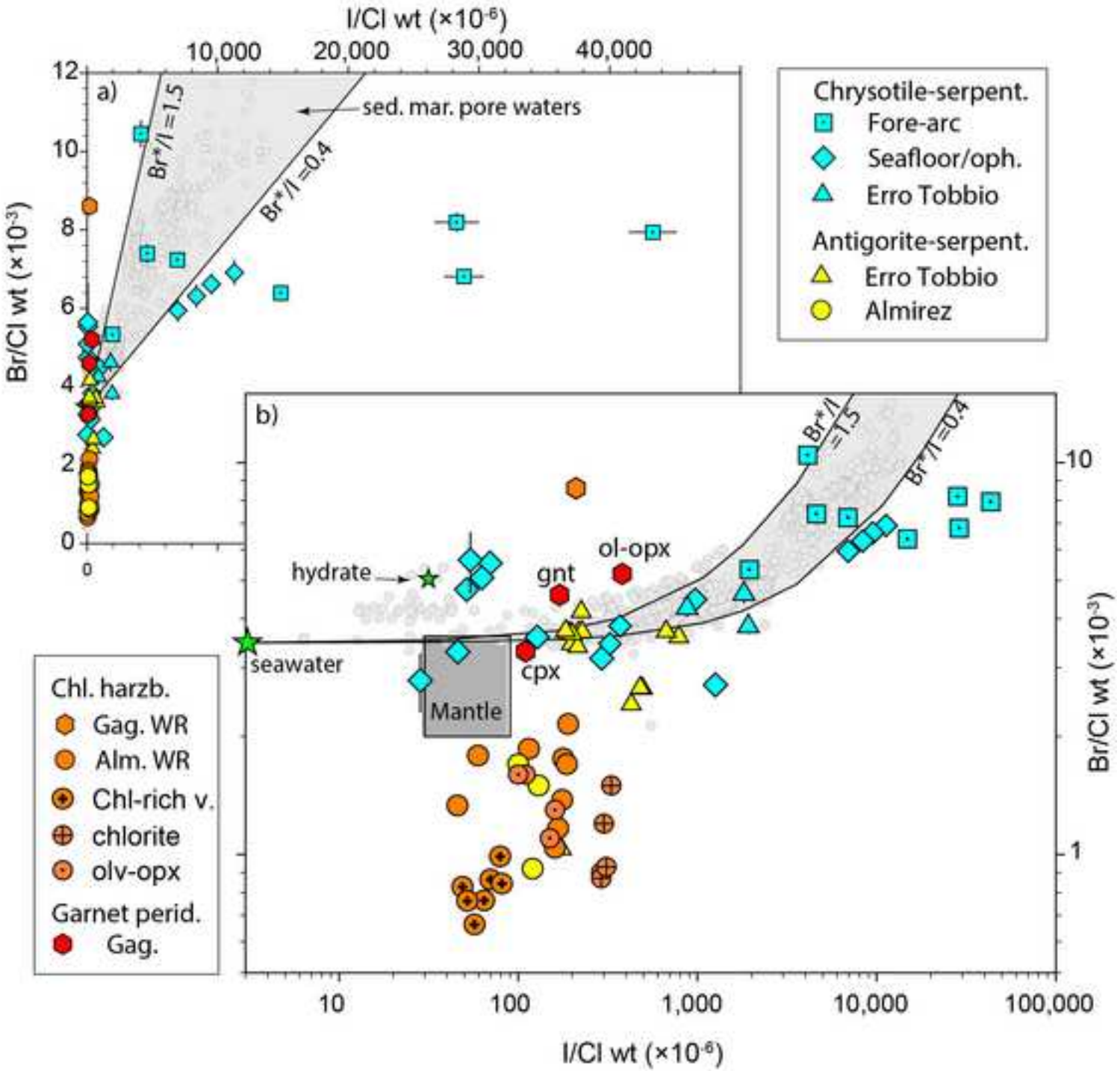

Figure
Click here to download high resolution image

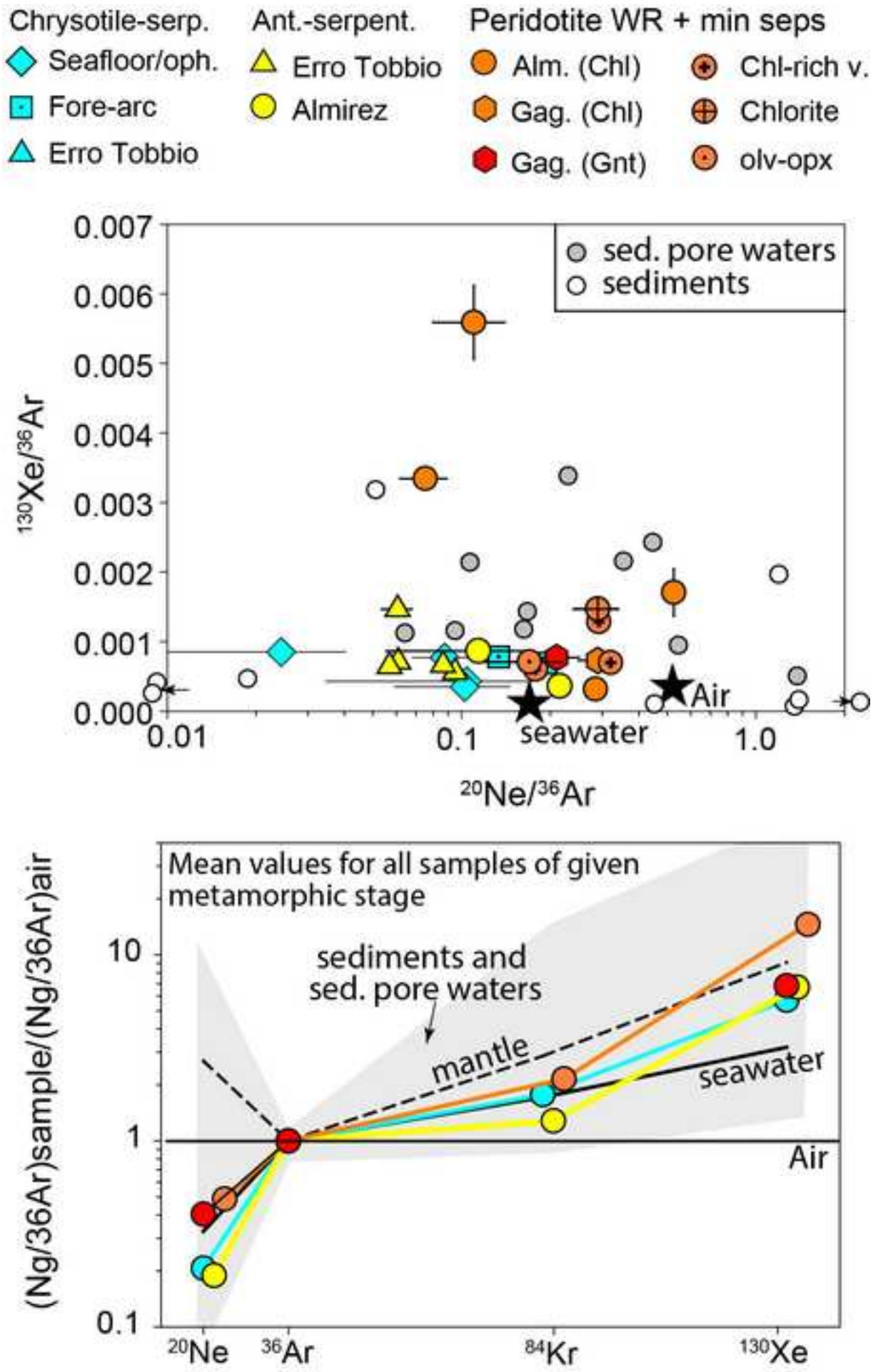

Figure

Click here to download high resolution image

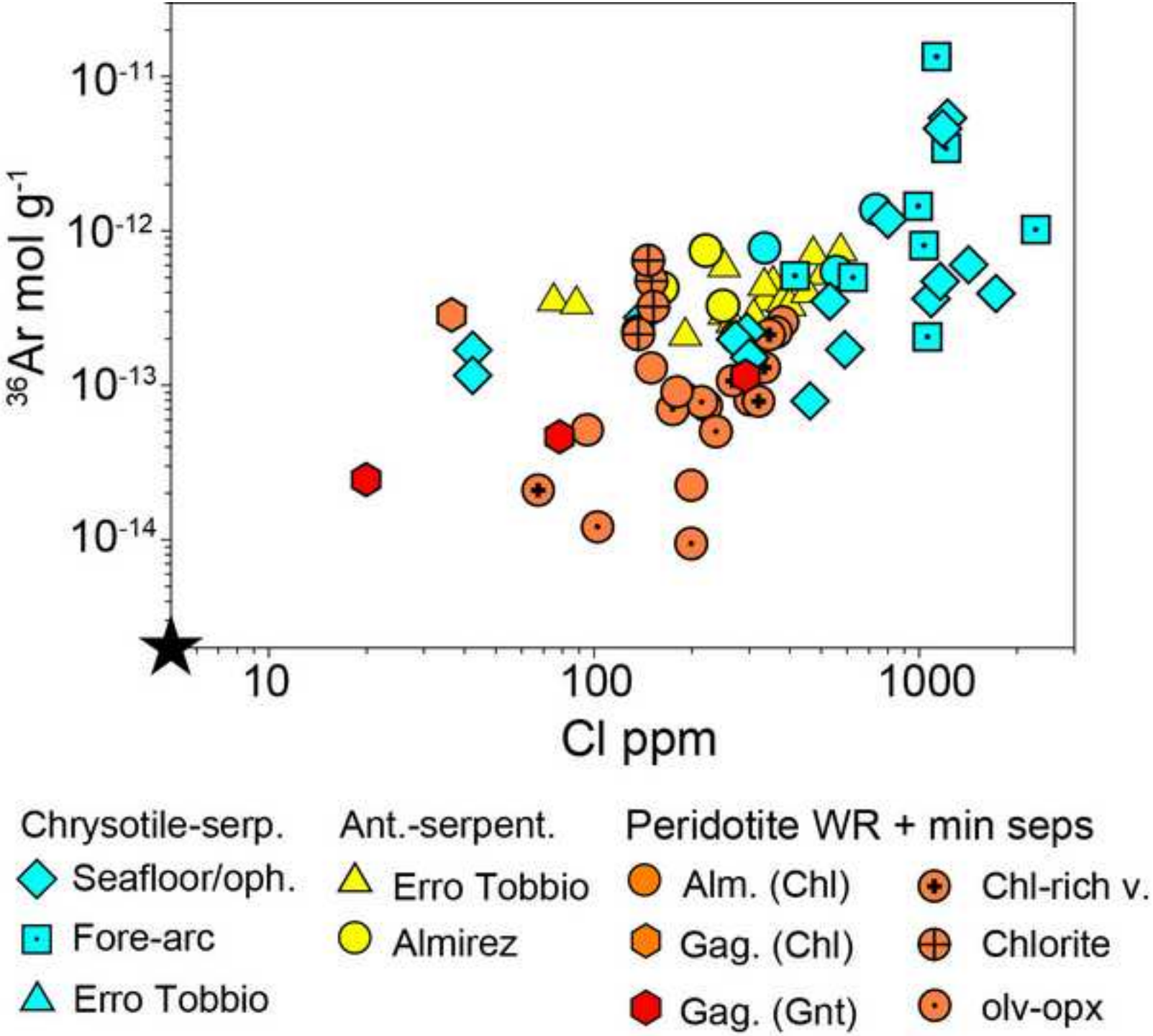

Figure
Click here to download high resolution image